




Effects of oxygen partial pressure on the electrical properties and phase transitions in (Ba,Ca)(Ti,Zr)O₃ ceramics

Wei Cai^{1,2,*} , Qianwei Zhang¹, Chuang Zhou¹, Rongli Gao^{1,2}, Fengqi Wang¹, Gang Chen^{1,2}, Xiaoling Deng^{1,2}, Zhenhua Wang^{1,2}, Nengyun Deng¹, Li Cheng¹, and Chunlin Fu^{1,2,*}

¹ School of Metallurgy and Materials Engineering, Chongqing University of Science and Technology, University Town, Shapingba District, Chongqing 401331, China

² Chongqing Key Laboratory of Nano/Micro Composite Material and Device, University Town, Shapingba District, Chongqing 401331, China

Received: 11 February 2020

Accepted: 2 May 2020

Published online:

11 May 2020

© Springer Science+Business Media, LLC, part of Springer Nature 2020

ABSTRACT

To enhance the piezoelectric responses, Ba_{0.85}Ca_{0.15}Zr_{0.1}Ti_{0.9}O₃ (BCZT) ceramics were fabricated by a sol–gel method in various sintering atmospheres. The effects of oxygen partial pressure on the microstructure and electrical properties of BCZT ceramics were systematically investigated. The samples sintered in air, O₂ and N₂ are the coexistence of the orthorhombic (O)-tetragonal (T) phase at room temperature. The phase transition temperature of the O–T phase of BCZT samples sintered in air, O₂ and N₂ is gradually closer to room temperature. The results of EDS, XPS and the activation energy confirm the significant effect of oxygen sintering atmosphere. BCZT samples sintered in oxygen atmosphere show excellent ferroelectricity ($2P_r = 31.62 \mu\text{C}/\text{cm}^2$, $2E_C = 3.46 \text{ kV}/\text{cm}$) and significantly enhanced piezoelectricity ($d_{33} = 604.3 \text{ pC}/\text{N}$, $d_{33}^* = 647.5 \text{ pm}/\text{V}$ and $k_p = 58\%$), resulting from the minimum oxygen vacancy, the phase transition temperature of O–T closer to room temperature and dense microstructure. These results demonstrate that adjusting oxygen partial pressure in sintering is an effective way to enhance the piezoelectric responses of BCZT ceramics.

Introduction

Pb(Zr,Ti)O₃ (PZT) materials are extensively used as ultrasonic transducers, sensors and actuators on account of their high piezoelectric constant ($d_{33} \sim 600 \text{ pC}/\text{N}$) [1, 2]. But the heavy use of lead

will bring serious environmental pollution. Hence, it is particularly important to discover lead-free candidates with superior piezoelectricity [3, 4]. Lead-free BaTiO₃ (BT) [5, 6]-, (Bi,Na)TiO₃ (BNT) [7, 8]- and (K,Na)NbO₃ (KNN) [9, 10]-based piezoceramics have been investigated. BaTiO₃-based ceramics have

Address correspondence to E-mail: caiwei_cqu@163.com; chlifu@126.com

become popular among these piezoelectric ceramics [11, 12]. In particularly, Liu and Ren discovered that the high piezoelectric constant ($d_{33} = 550 \sim 620$ pC/N) of $\text{Ba}_{1-x}\text{Ca}_x\text{Zr}_y\text{Ti}_{1-y}\text{O}_3$ ($x = 0.15$, $y = 0.1$, short for BCZT) piezoceramics stems from a tricritical point-type morphotropic phase boundary (MPB) [13].

The optimization of preparation process [14–16], crystallographic texture [17, 18] and doping (LiTaO₃, Sn⁴⁺, Hf⁴⁺, Mn⁴⁺, Nd³⁺, et al.) [19–23] have been used to enhance the piezoelectricity of BCZT ceramics. It is hard to obtain excellent piezoelectric response ($d_{33} > 550$ pC/N) in BCZT ceramics, and an important reason may be that the phase transition temperature of rhombohedral-tetragonal or orthorhombic-tetragonal is above the room temperature [13, 24, 25]. Therefore, if the phase transition temperature of BCZT ceramics could shift to room temperature, its piezoelectric properties will be further improved. There is no doubt that the phase transition temperature of BCZT ceramics is influenced by grain size [26–28]. In our previous study, the construction of the O-T phase boundary near room temperature has been realized by gaining super grain size ($> 50 \mu\text{m}$), which leads to the high piezoelectric coefficient ($d_{33} = 585.6$ pC/N, $d_{33}^* = 898$ pm/V) of BCZT ceramics [27]. Moreover, doping is a common method to shift the phase transition point of BCZT ceramics. Wu et al. shifted the tricritical point to room temperature by adding ZnO and improved the piezoelectric response ($d_{33} \sim 521$ pC/N) of BCZT ceramics [25]. Zhao et al. found that the introduction of $(\text{Cu}_{1/3}\text{Nb}_{2/3})_x\text{O}_3$ in BCZT ceramics could obtain a room-temperature polymorphic phase transition point and enhance its piezoelectric responses [29]. Cu/Y-coping BCZT ceramics could make the Curie temperature increase by 5–15 °C and lead to the coexistence of the O-T phase close to room temperature, which resulted in an improved piezoelectric property ($d_{33} = 552$ pC/N) [30]. In general, the introduction of acceptor dopants in BCZT ceramics will bring about the formation of oxygen vacancies. Besides acceptor doping, it is easy to form the oxygen vacancies during the high-temperature sintering. Domain-stabilizing defect pairs will form through the interaction of oxygen vacancies and cations [22, 31]. An inner bias field caused by the formed defect pairs leads to the reduction in the polarization rotation and the motion of domain wall [32], resulting in the decrease in the piezoelectric coefficient. In other words, the existence of oxygen vacancies may

unfavorable for excellent piezoelectric properties of BCZT ceramics. However, Zhang et al. fabricated BCZT piezoceramics in N₂ and air atmospheres, respectively, and found that the sintering atmosphere has no significant effects on the piezoelectric coefficient and phase structure [33]. Thus, it seems rather confusing to understand the effects of oxygen vacancy. Besides, the correlations between the oxygen vacancy and phase structure in other piezoelectric ceramics such as $\text{PbZr}_{1-x}\text{Ti}_x\text{O}_3$ and $\text{PbZn}_{1/3}\text{Nb}_{2/3}\text{O}_3$ -based materials have been investigated, and the results show that the oxygen vacancy significantly influences the phase structure and electrical performances [34, 35]. Therefore, the effects of oxygen vacancy on the phase structure and electrical properties of BCZT ceramics need to be further clarified.

In summary, the phase coexistence near room temperature of BCZT ceramics is favorable to the improvement of piezoelectricity. The phase structure and electrical properties of BCZT ceramics should be influenced by oxygen vacancy. Therefore, adjusting oxygen partial pressure in sintering for BCZT ceramics is expected to further improve the piezoelectric responses by affecting phase structure and reducing oxygen vacancy. Besides, the solid-state method is not easy to obtain the piezoelectric ceramics with homogeneous composition, and the sol-gel method has been widely used to fabricate BaTiO₃-based ceramics because of its obvious advantages such as accurate stoichiometric ratio and compositional homogeneity [36, 37]. To figure out the effects of oxygen vacancy and improve the piezoelectric responses, BCZT ceramics were prepared by chemical synthesis method and sintering in various atmospheres, and the influences of oxygen vacancy on its microstructure and electrical properties were systematically investigated.

Experimental

The synthesis process of BCZT powders is shown in Fig. 1. The experimental details from raw materials to dry gel have been described in our previous paper [27]. Finally, the dry gel was calcined at 800 °C for 2 h to obtain BCZT powders.

BCZT powders were pressed into the pellets at 16 MPa and then sintered at 1500 °C for 10 h in various atmospheres to get BCZT ceramics. BCZT-

Air, BCZT-O₂ and BCZT-N₂ represent BCZT ceramics sintered in air, O₂ and N₂, respectively.

The XRD (SmartLab-9, Rigaku, Japan) was applied to obtain the phase structure of samples. The surface morphology of samples was characterized by SEM (S-3700 N, Hitachi, Japan). The elemental analysis of BCZT ceramics was carried out by EDS (ApolloII, EDAX, USA). The XPS (K-Alpha, Thermo Fisher Scientific, USA) was applied to oxygen elemental analysis. The variations of dielectric properties with the temperature in a range of 20–200 °C and the impedance spectroscopy of BCZT ceramics were tested by an LCR meter (HP 4980A, Agilent, USA). The ferroelectric test system (TF2000E, aixACCT Germany) was applied to obtain ferroelectric properties and strain behaviors of the samples under the electric field. The ceramic sample was poled under the DC field of 20 kV/cm for 20 min at 25 °C, and its quasi-static piezoelectric constant (d_{33}) was measured by a quasi-static d_{33} m (ZJ-4AN, Institute of Acoustics, China). The planer mode electromechanical coupling coefficient (k_p) was obtained by an impedance analyzer (HP 4294A, Agilent, USA)

Results and discussion

Microstructure

Figure 2 exhibits the XRD patterns of all BCZT ceramics. There is no impurity observed in all samples, indicating that all samples are pure phase. To reveal the phase structure of BCZT ceramics fabricated in different sintering atmospheres, the fine scanning XRD patterns around 45° and Rietveld refinement of crystal structure were performed (see Fig. 2 and insert in Fig. 2a–c). Generally speaking, the

diffraction peaks of barium titanate around 45° may be (200)_R of rhombohedral phase, (022)/(200)_O of orthorhombic phase or (002)/(200)_T of tetragonal phase [16]. The hidden diffraction peaks around 45° in all samples were determined by Gaussian fitting and comparing to the diffraction peaks corresponding to the tetragonal, rhombohedral and orthorhombic phase of BaTiO₃ standard cards [15, 38, 39]. The fitting results show that the BCZT samples sintered in air, O₂ and N₂ are the coexistence of the O–T phase, and the content of the O and T phase for different samples is different, indicating that sintering atmosphere has significant effects on the phase content. The content of the O and T phases in all BCZT ceramics is given in Table 1. The content of the O phase of BCZT samples sintered in air, O₂ and N₂ gradually decreases, and the content of the T phase gradually increases, indicating that O–T phase coexistence of BCZT ceramics gradually becomes more uniform. Furthermore, there is an interesting phenomenon that the intensity of (200) peak around 45° of BCZT samples sintered in O₂, air and N₂ gradually increases, and (200) peak of BCZT-N₂ samples becomes the strongest, which indicates that BCZT ceramics gradually show (100) orientation as the oxygen content of sintering atmosphere decreases. The result may ascribe to the competitive growth mode among various orientations at different sintering atmospheres [40–42]. Zhang [43] and Yang [42] also found a similar phenomenon in other ferroelectric materials (Bi_{0.5}Na_{0.5}TiO₃ and Sr₂Bi₄Ti₅O₁₈ sintered in N₂ atmosphere). The orientation may be due to that the different surface energy of grain growth leads to the anisotropy of nucleation and growth rates of different directions when the samples are sintered in various atmospheres [44]. Furthermore,

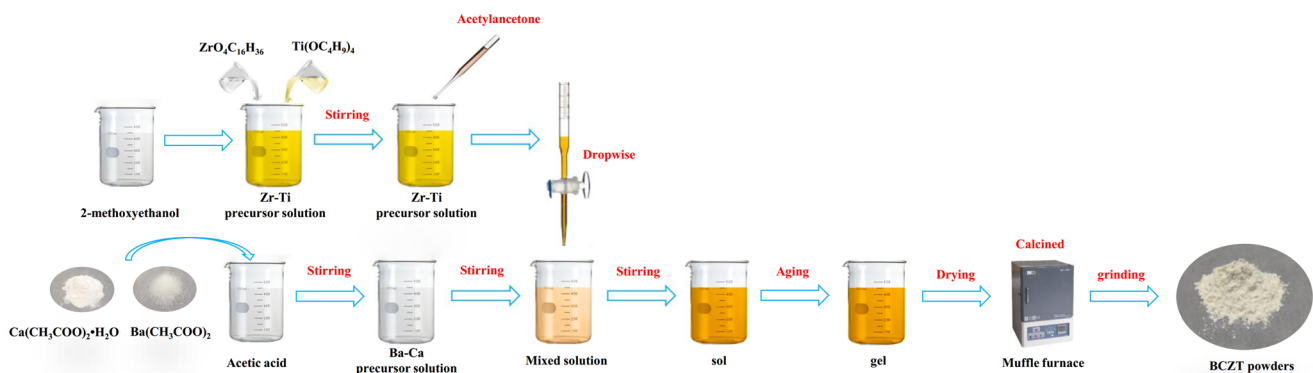


Figure 1 Synthesis process of BCZT powders.

Figure 2 XRD patterns and Rietveld refinement of BCZT samples: **a** air, **b** O₂ and **c** N₂.

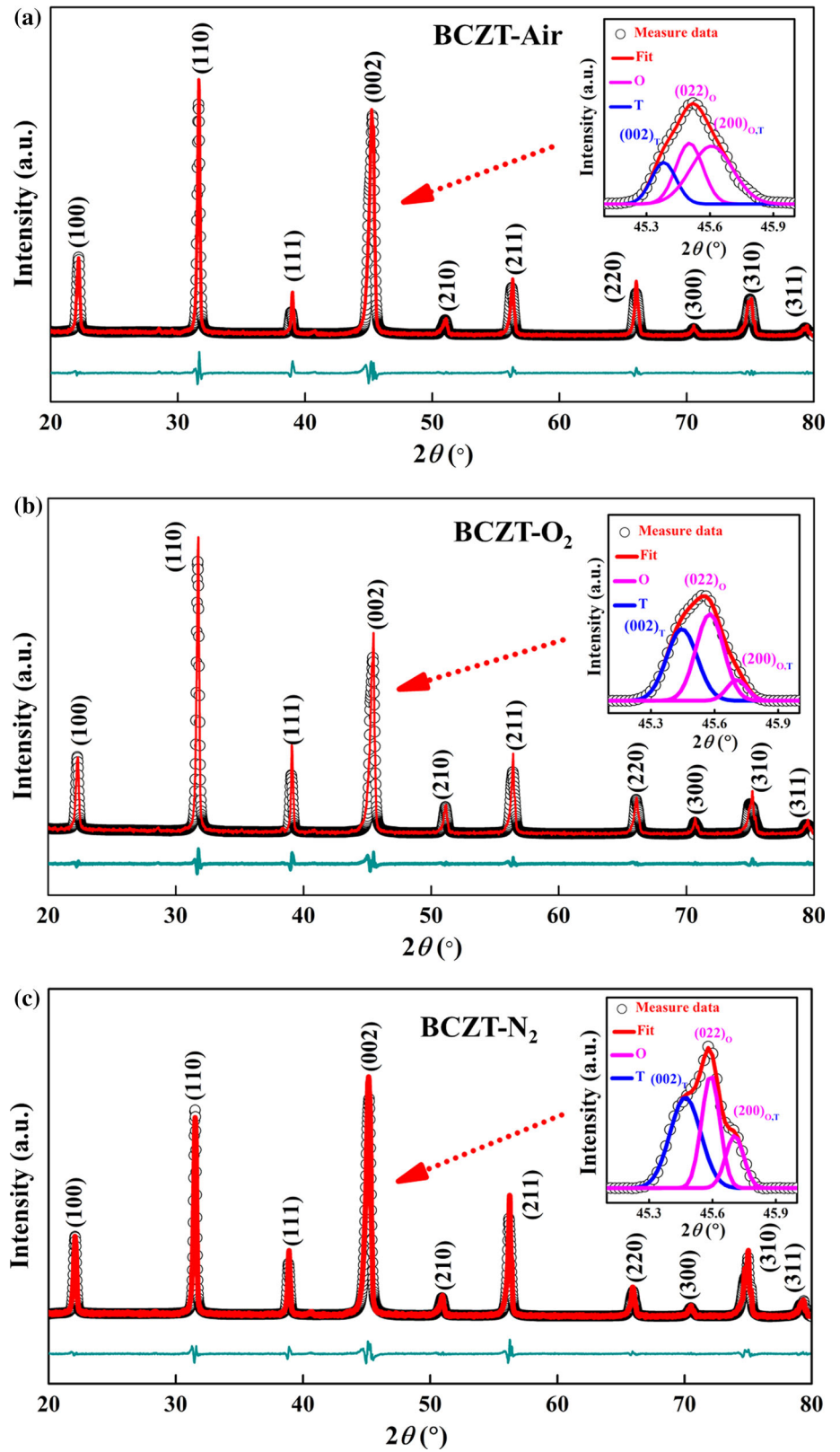


Table 1 Lattice parameters of BCZT ceramics sintered in different atmospheres

Samples	Lattice parameters				Phase content (%)		R_{wp} (%)	R_p (%)			
	Tetragonal phase		Orthorhombic phase		O	T					
	a (nm)	c (nm)	Cell volume (nm ³)	Tetragonality (c/a)	a (nm)	b (nm)			c (nm)		
Air	0.3984	0.4002	0.0635	1.0046	0.3992	0.5656	0.5671	80	20	7.91	5.91
O ₂	0.3989	0.4008	0.0638	1.0048	0.3998	0.5663	0.5698	56	44	9.74	7.42
N ₂	0.3982	0.4002	0.0634	1.0050	0.3989	0.5643	0.5662	52	48	6.34	5.14

Table 1 shows the lattice parameters of all samples obtained by the Rietveld refinement method. The result shows that the lattice constants of BCZT samples sintered in O₂, air and N₂ gradually decrease, which attributes to the increase in the oxygen vacancy concentration.

The SEM images and grain size distribution of all samples were obtained and are shown in Fig. 3. Firstly, BCZT-O₂ and BCZT-N₂ samples show more compact than BCZT-Air samples. The relative density of BCZT samples sintered in air, O₂ and N₂ is 94.7%, 97.6% and 96.9%, respectively, indicating that the oxygen-enriched sintering is conducive to getting dense BCZT samples. Secondly, the samples sintered in air, O₂ and N₂ have the average grain size (G_a) of 37.8 μm , 32.6 μm and 13.5 μm , respectively. In general, the oxygen vacancies are propitious to the growth of grain in the ceramic sample, and more oxygen vacancies lead to the larger grain size. Therefore, the G_a of BCZT-Air samples with relatively higher oxygen vacancy concentration is larger than that of BCZT-O₂ samples with lower oxygen vacancy concentration. But the G_a of BCZT-N₂ samples with the maximum oxygen vacancy concentration among all the samples is the smallest. It reveals that the nitrogen atmosphere goes against the growth of BCZT ceramics, which may be due to the existence of a small amount of grain boundary pinning phase. Tkach [45] and Zhang [46] also found that a similar phenomenon that the G_a of some ceramics such as SrTiO₃ and Ca_{0.6}Sr_{0.4}TiO₃ sintered in N₂ is smaller than that of the sample sintered in air. Moreover, compared to BCZT-O₂ and BCZT-N₂ samples, the grain of BCZT-Air sample is more uniform (see Fig. 3d–f).

To find out the composition difference of the samples sintered in various atmospheres, the EDS analysis of all ceramic samples is given in Fig. 4. Although the content of oxygen as a light element

determined by EDS is not accurate enough, the comparison of oxygen content in BCZT ceramics sintered in various atmospheres is still meaningful. The oxygen content of BCZT-O₂, BCZT-Air and BCZT-N₂ ceramics gradually decreases, suggesting the gradually increased oxygen vacancy concentration.

To further confirm the difference in oxygen vacancy concentration of the samples, the XPS measurement was taken. The typical XPS survey spectrum (shown in Fig. 5a) suggests that there are barium (Ba), calcium (Ca), zirconium (Zr), titanium (Ti), oxygen (O) and carbon (C) in BCZT-O₂ ceramics. The existence of carbon is due to atmosphere contamination [47]. The O1s spectra of all BCZT samples were fitted and are shown in Fig. 5b–d. The unsymmetrical O1s peak was fitted into three component peaks with specific positions. The O1s(I) peak (529.31 eV) represents lattice oxygen ions (O²⁻), the O1s(II) peak (530.95 eV) represents O₂⁻/O⁻ ions induced by oxygen vacancy and the O1s(III) peak (531.74 eV) relates to the organic oxygen on the surface of the samples [47]. The O1s spectra of the samples sintered in different atmospheres exhibit obvious differences except for the area of O1s(III) peak. The area of O1s(I) peak in the sample sintered in O₂ is the maximum, and the area of O1s(II) peak in BCZT sample sintered in O₂ is the minimum, indicating that the oxygen vacancy compensation has been realized by oxygen-enriched sintering. The XPS result is consistent with the EDS results.

Dielectric properties

Figure 6 shows the variations of the dielectric constant and loss of BCZT samples sintered in various atmospheres with the temperature. Firstly, there is a distinct peak of dielectric constant between 80 °C and

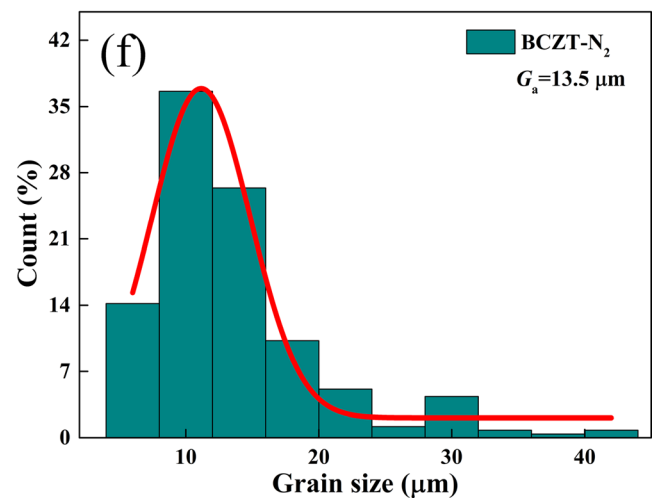
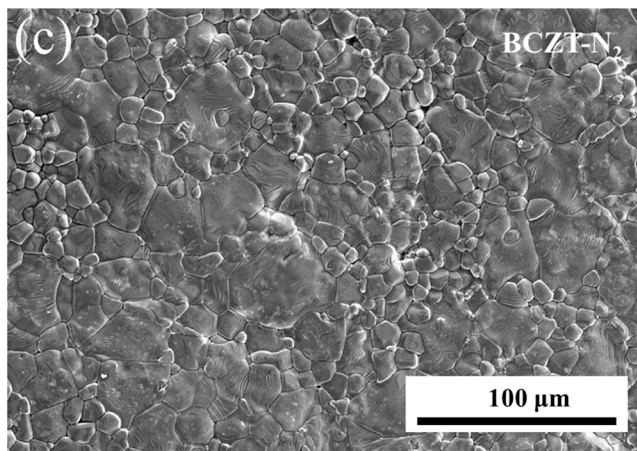
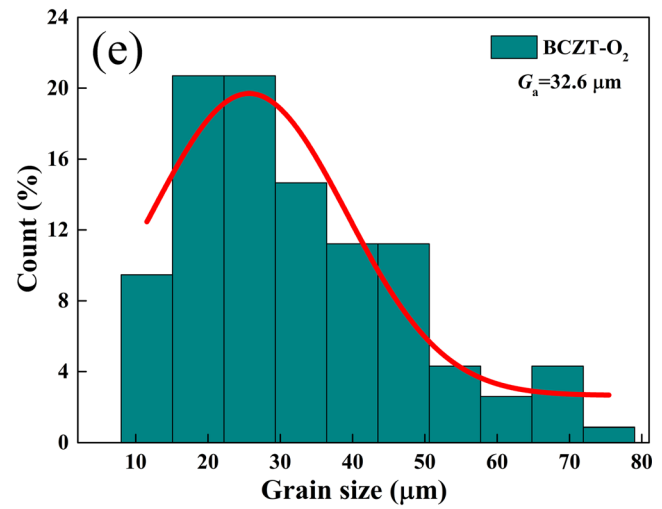
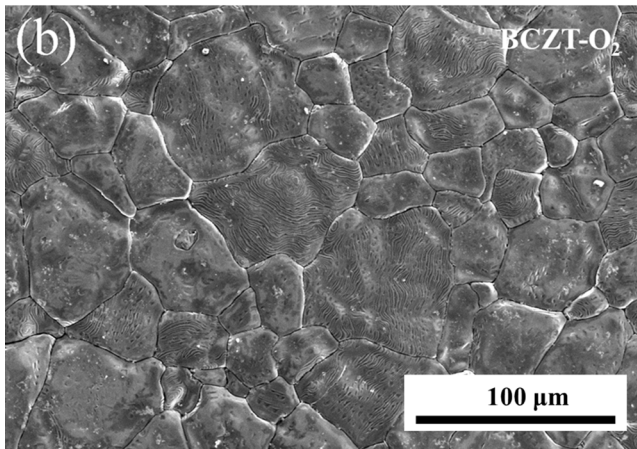
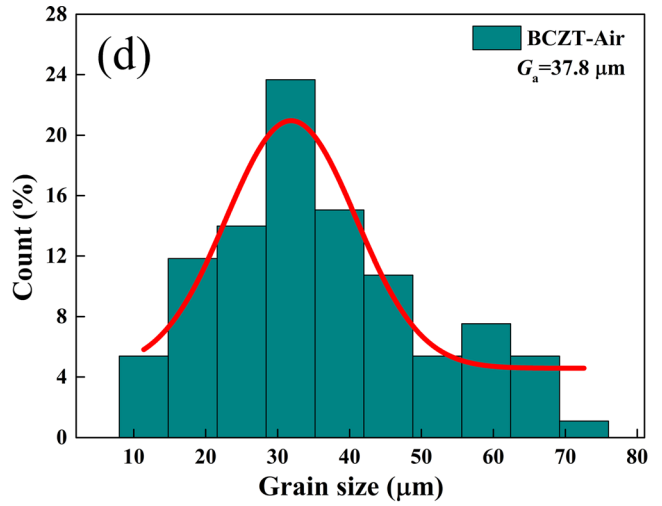
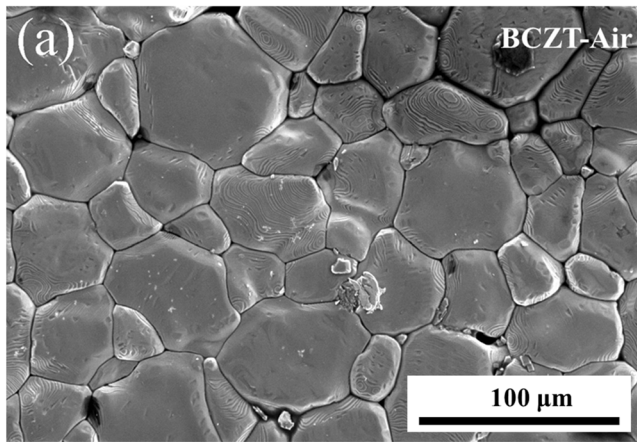


Figure 3 Surface morphology and grain distribution of the samples sintered in various atmospheres: **a, d** air, **b, e** O₂ and **c, f** N₂.

90 °C corresponding to the Curie temperature (T_C) of tetragonal-cubic phase transition in all BCZT samples. All samples show a relatively flat peak of

dielectric constant near 30 °C. According to the analysis of XRD results, there is the coexistence of the O and T phase for BCZT samples sintered in air, O₂

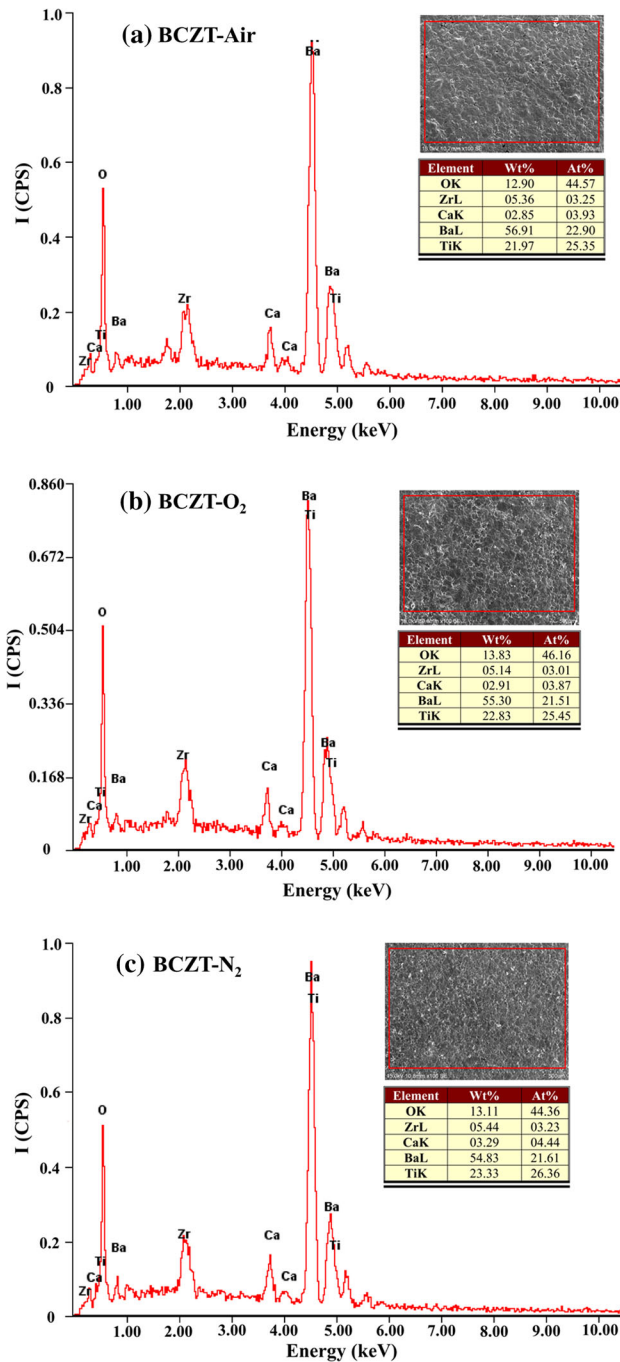


Figure 4 EDS results of the samples sintered in various atmospheres: **a** air, **b** O₂ and **c** N₂.

and N₂ at room temperature. Based on the above results, the peak of dielectric constant near 30 °C corresponds to the phase transition behavior of O–T [48], and T_{O-T} (the transition temperature of O–T phase) of BCZT-Air, BCZT-O₂ and BCZT-N₂ samples is 32 °C, 30 °C and 28 °C, respectively. Secondly, as the frequency increases, the Curie temperature (T_C)

of all BCZT samples remain unchanged, indicating no frequency dispersion. But the dielectric constant peak (ϵ_m) of all samples gradually reduces with the increase in frequency, which results from the different relaxation behaviors of polarization mechanisms (dipole, electron, ionic and space-charge polarization) [27, 49]. Moreover, there is a dielectric loss peak near the Curie temperature corresponding to phase transition in all BCZT ceramics.

Figure 7 shows the variations of dielectric constant and loss of all BCZT samples with temperature measured at 1 kHz, and the maximum dielectric constant and room-temperature dielectric loss are shown in Table 2. Firstly, the T_C of BCZT-Air, BCZT-O₂ and BCZT-N₂ samples is 89.1 °C, 86 °C and 80.9 °C, respectively. The combined action of internal stress and tetragonality (c/a) leads to the change of T_C . On the one hand, the T_C of piezoceramics with the smaller grain size is lower [50, 51], resulting from the higher internal stress of fine grain because of lacking 90° ferroelectric domain walls [52]. On the other hand, the T_C of BaTiO₃-based ceramics falls with the decrease in the tetragonality [53]. The previous XRD and SEM results reveal that the tetragonality (shown in Table 1) of BCZT-Air, BCZT-O₂ and BCZT-N₂ samples increases little by little, while the grain size gradually decreases. The gradually decreased T_C of our BCZT samples sintered in air, O₂ and N₂ indicates that the grain size has a greater impact on the T_C than tetragonality. The change of T_{O-T} of our BCZT samples is similar to the Curie temperature. Secondly, the ϵ_m of BCZT samples sintered in air, O₂ and N₂ is 22167, 25372 and 20992, respectively. The ϵ_m of BCZT-N₂ samples is the minimum among all samples, resulting from its obvious grain refinement and increased oxygen vacancy concentration. On the one hand, oxygen vacancies would interact with cations to form domain-stabilizing defect pairs, which could prohibit the movement of ferroelectric domain walls so that the polarization decreases [22]. On the other hand, the grain refinement of ferroelectric ceramics results in the decreased total contribution of grains to the polarization [54] in BCZT-N₂ ceramics. Thirdly, the dielectric loss of the sample sintered in air is slightly higher than that of the samples sintered in O₂ and N₂. Despite the higher oxygen vacancy concentration in BCZT-N₂ samples, its better densification has greater effects on dielectric loss and leads to its lower dielectric loss. Moreover, the maximum dielectric

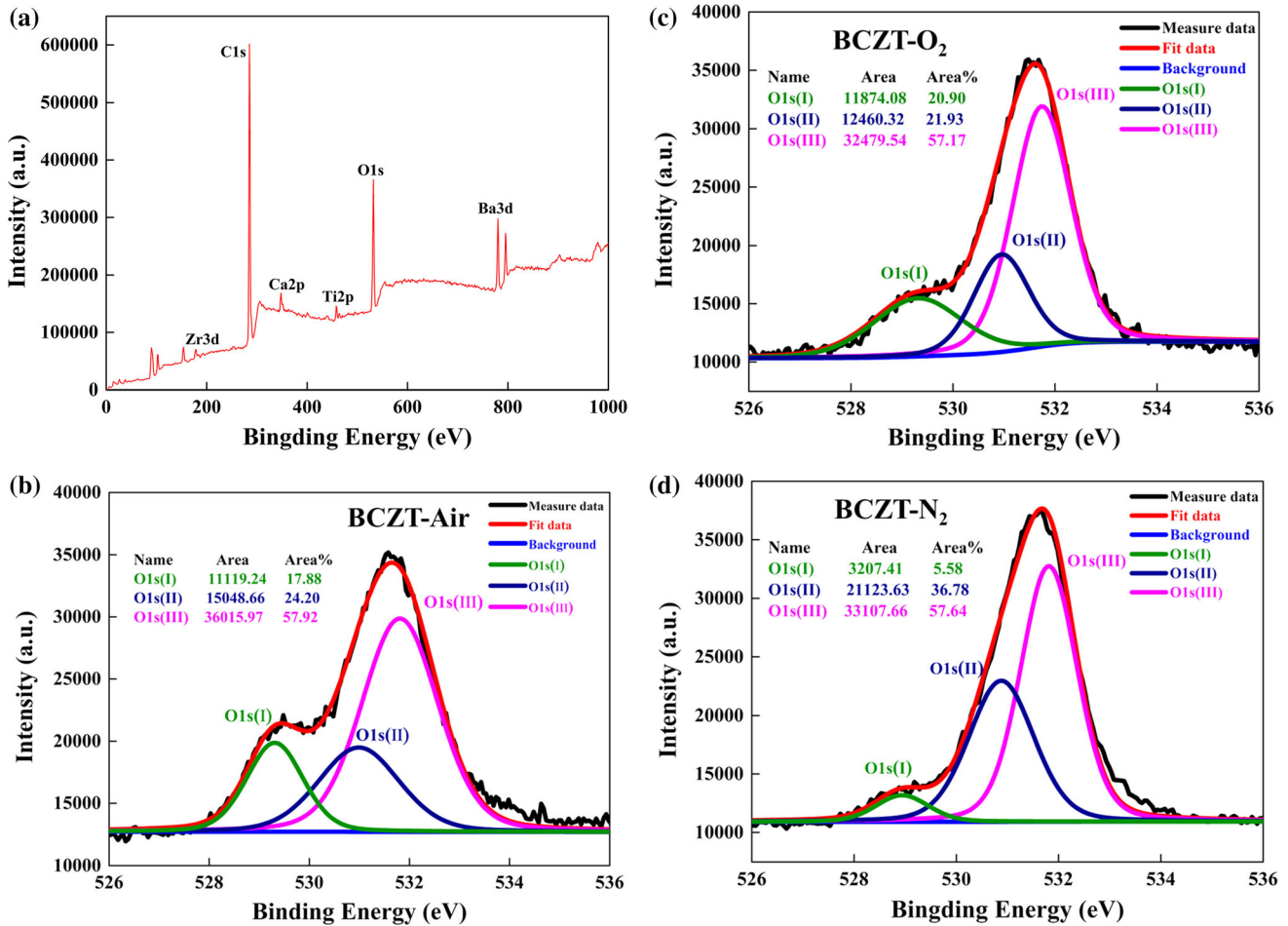


Figure 5 aXPS survey spectrum of BCZT-O₂ samples and high-resolution O1s spectrum of the samples sintered in various atmospheres: b air, c O₂ and d N₂.

constant peak of all BCZT samples shows obvious broadening, indicating the diffuse phase transition characteristic.

The modified Curie–Weiss law has been used to characterize the diffuse phase transition:

$$\frac{1}{\epsilon_r} - \frac{1}{\epsilon_m} = \frac{(T - T_m)^\gamma}{C'} \quad (1)$$

where γ is the diffuseness constant and C' is constant. The plots of $\ln(1/\epsilon - 1/\epsilon_m)$ and $\ln(T - T_m)$ of all samples exhibit obvious linear characteristics (shown in Fig. 8). The slope (γ) of linear fitting plots for BCZT-Air, BCZT-O₂ and BCZT-N₂ ceramics is 1.56, 1.57 and 1.61, respectively, indicating that the diffuse phase transition gradually enhances. The enhanced diffuse phase transition of BCZT-N₂ samples results from its obvious grain refinement.

Ferroelectric properties

Figure 9 shows the polarization hysteresis loops (P – E) and switching current curves (I – E) of BCZT samples measured at 10 Hz. The coercive electric field ($2E_C$) and remnant polarization ($2P_r$) are given in Table 2. Firstly, the P – E loops of all samples show good rectangularity (especially for BCZT-O₂), indicating that they have excellent ferroelectric properties. Two obvious peaks near the coercive electric field in the I – E curves of all BCZT samples correspond to the switching of ferroelectric domains. Secondly, BCZT-O₂ samples have the highest remnant polarization ($2P_r = 31.62 \mu\text{C}/\text{cm}^2$) and the lowest coercive electric field ($2E_C = 3.46 \text{ kV}/\text{cm}$) among all the samples. The P_r and E_C of our BCZT ceramic sample are higher and lower than that reported in the studies [16, 19, 20, 48], indicating the excellent ferroelectricity of our BCZT-O₂ samples. The

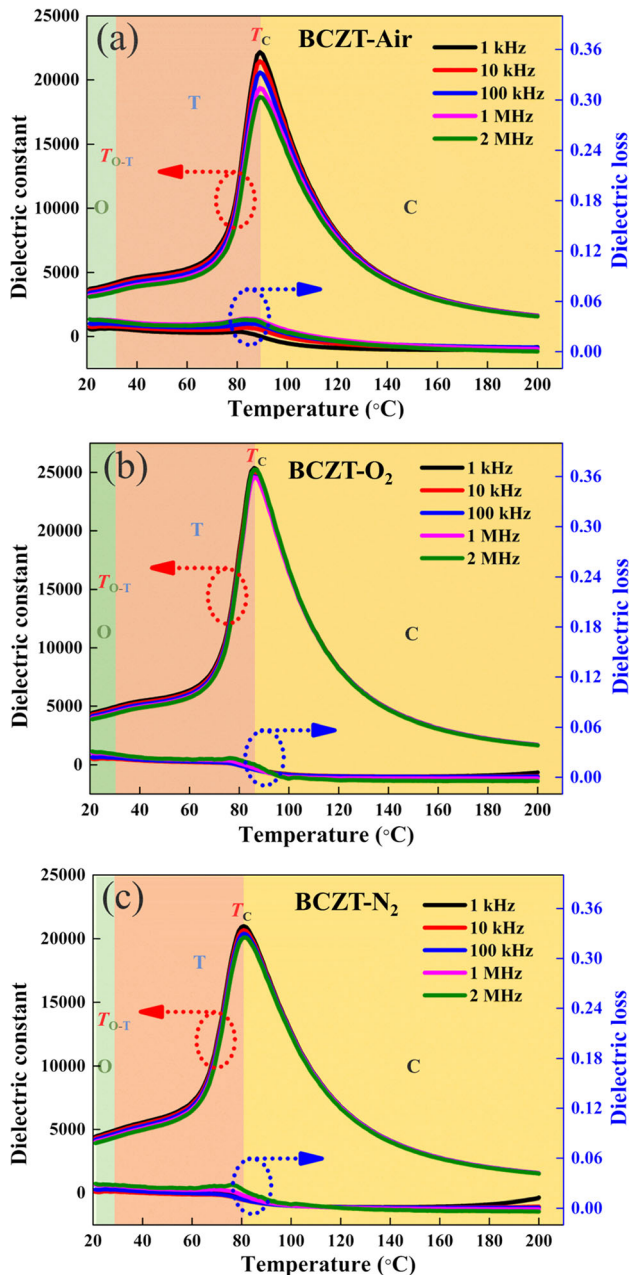


Figure 6 Variations of dielectric constant and loss of BCZT samples sintered in various atmospheres with the temperature: **a** air, **b** O₂ and **c** N₂.

ferroelectricity of BCZT ceramics is affected by many factors, such as grain size and oxygen vacancy. In general, the increased energy barrier with the grain refinement make the ferroelectric domain more difficult to switch so that the smaller grain size results in a higher coercive electric field [55, 56], and the greater contribution of grain to the polarization than grain boundary leads to the lower P_r of the sample with the smaller grain size [57]. Moreover, the formed defect

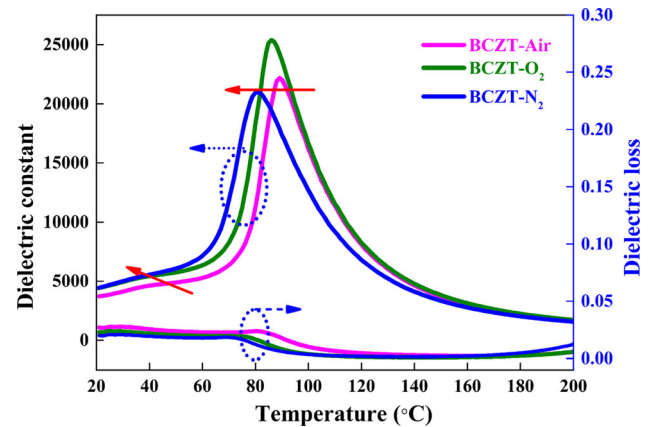


Figure 7 Variations of dielectric properties of BCZT samples sintered in various atmospheres with the temperature measured at 1 kHz.

Table 2 Remnant polarization ($2P_r$), coercive electric field ($2E_C$), the maximum dielectric constant (ϵ_m), room-temperature dielectric loss ($\tan\theta$), quasi-static piezoelectric coefficient (d_{33}), dynamic piezoelectric coefficient (d_{33}^*) and electromechanical coupling coefficient (k_p) of BCZT ceramics sintered in different atmospheres

Samples	BCZT-Air	BCZT-O ₂	BCZT-N ₂
$2P_r$ ($\mu\text{C}/\text{cm}^2$)	25.94	31.62	27.55
$2E_C$ (kV/cm)	4.76	3.46	3.59
ϵ_m	22167	25372	20992
$\tan\theta$	0.027	0.023	0.020
d_{33} (pC/N)	528.4	604.3	558.2
d_{33}^* (pm/V)	481.5	647.5	627
k_p (%)	48	59	52

pairs caused by oxygen vacancies can hinder the motion of the ferroelectric domain (called as domain wall pinning effect) so that the coercive electric field increases and the remnant polarization decreases [22]. But our results are different. For example, BCZT-N₂ samples with the obviously smaller grain size and higher oxygen vacancy concentration have higher P_r and lower E_C than that of BCZT-Air samples. It suggests that there are other more important influencing factors expect for grain size and domain wall pinning effect on the ferroelectricity for our samples. T_{O-T} corresponding to the phase transition of O-T phase of BCZT-O₂ and BCZT-N₂ ceramics is closer to room temperature than that of BCZT-Air ceramics according to the above-mentioned results (shown in Fig. 6). As everyone knows, the polarization anisotropy close to the phase transition almost disappears,

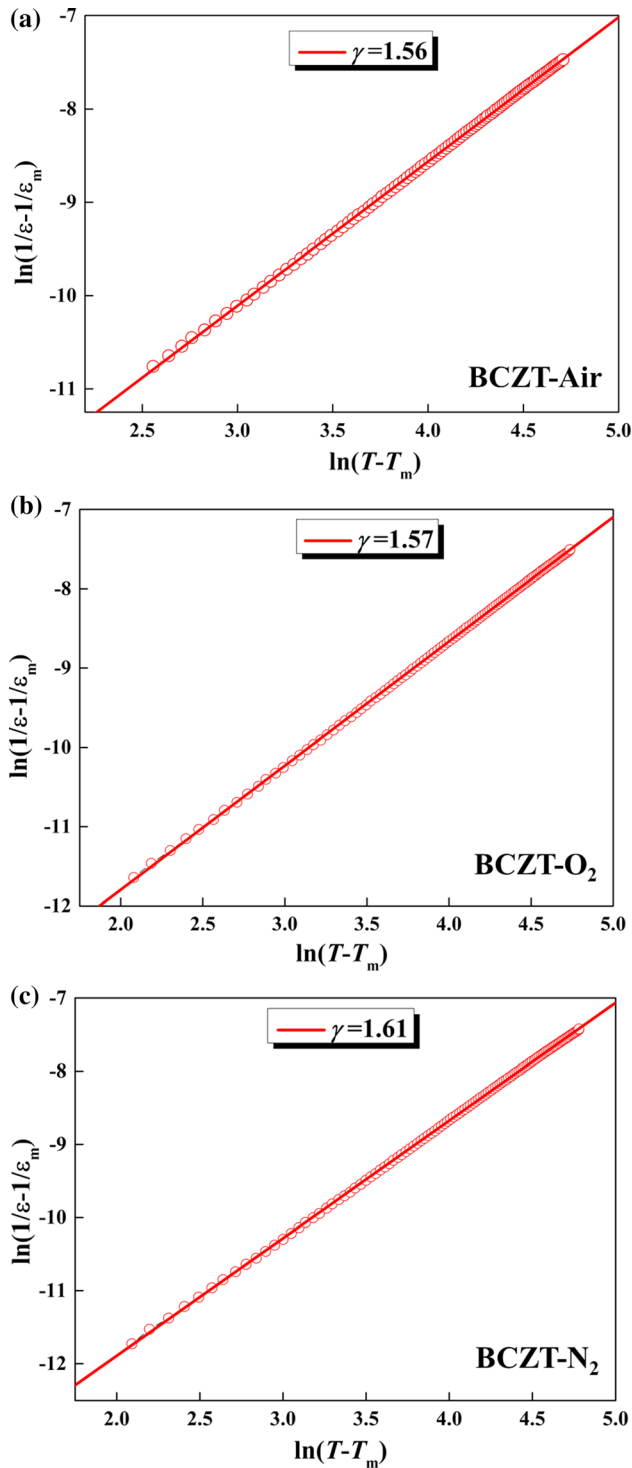


Figure 8 $\ln(1/\epsilon - 1/\epsilon_m)$ and $\ln(T - T_m)$ curves of BCZT samples: **a** air, **b** O_2 and **c** N_2 .

which is conducive to the polarization rotation and then results in the decreased coercive electric field and increased polarization [13]. Therefore, for our BCZT samples, the O-T phase transition near room

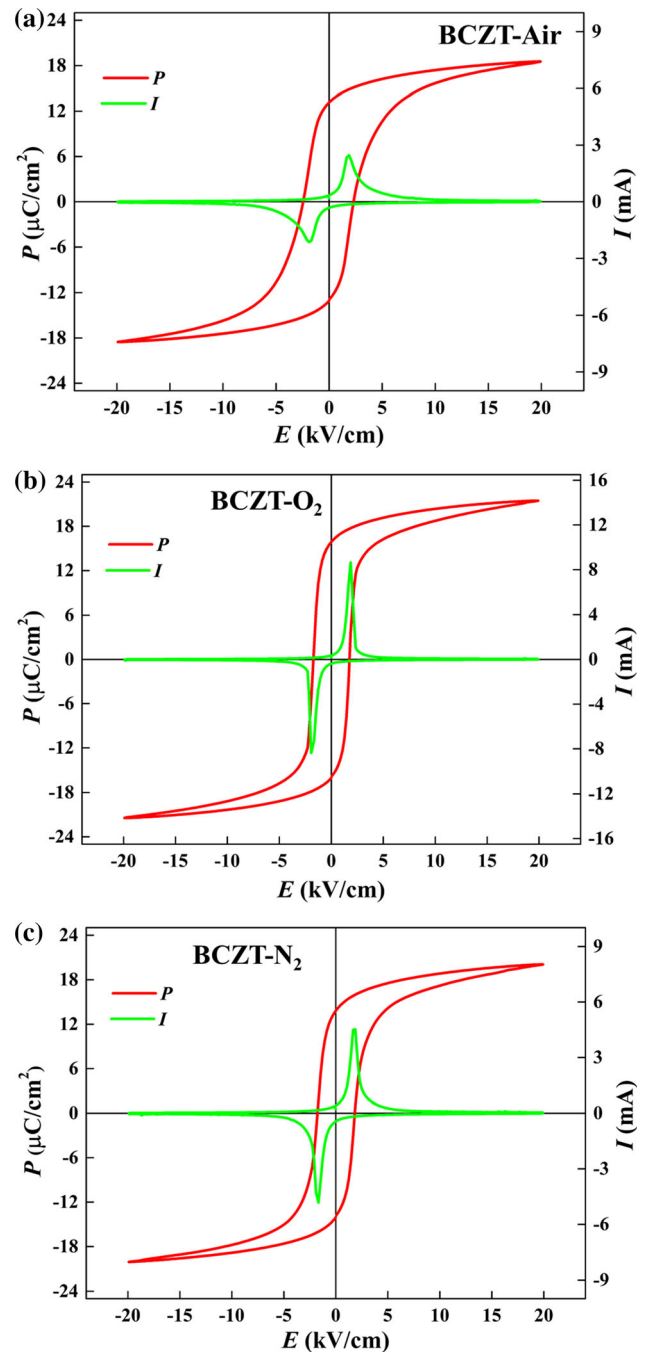


Figure 9 Room-temperature P - E and I - E curves of the samples: **a** BCZT-Air, **b** BCZT- O_2 and **c** BCZT- N_2 .

temperature has greater influences on the remnant polarization and coercive electric field than grain size and domain wall pinning effect caused by oxygen vacancy. It results in the superior room-temperature ferroelectricity of BCZT- O_2 and BCZT- N_2 ceramics with the smaller grain size. Furthermore, the maximum remnant polarization of BCZT- O_2 ceramics is

also closely related to the best densification and the least oxygen vacancy concentration.

Impedance properties

Impedance spectroscopy can be applied to find out the contributions of grain and grain boundary to the electrical responses. To analyze the conduction mechanisms, the real part of complex impedance (Z') of BCZT samples as a function of frequency measured at different temperatures (300 ~ 500 °C) is given in Fig. 10. Firstly, the Z' of all BCZT samples reduces with the increase in the frequency and the rise of temperature, indicating that the conductivity of all BCZT samples gradually enhances. Moreover, there is no significant change in the Z' of all BCZT samples with the temperature at higher frequency (> 50 kHz). Secondly, the Z' of BCZT samples sintered in air, O₂ and N₂ gradually decreases, indicating that the insulating property weakens. The variation of Z' of BCZT samples with the sintering atmosphere is consistent with that of its grain size. In general, the insulating property of grain in ferroelectric ceramics is better than that of grain boundary [46, 58, 59]. In other words, the ceramics with the larger grain size should exhibit better insulating properties. Moreover, the higher oxygen vacancy concentration of BCZT-N₂ samples makes its insulating property decrease. Therefore, the gradually reduced insulating property of BCZT-Air, BCZT-O₂ and BCZT-N₂ ceramics stems from the interaction of grain size and oxygen vacancy.

Figure 11 shows the imaginary part of impedance (Z'') of BCZT samples as a function of frequency at different temperatures. Firstly, the Z'' of all BCZT ceramics displays peak value (the maximum of Z'') with the changing of frequency. The decreased maximum Z'' of all BCZT samples with the rise of temperature suggests that the insulating property gradually reduces. The result is consistent with that of real Z' . Secondly, the peak of Z'' of all BCZT sample shifts to the higher-frequency region and gradually widens as the temperature rises. The result further proves that there is a relaxation phenomenon in all BCZT ceramics [60]. Finally, the electrical conductivity of BCZT samples sintered in N₂ is superior to that of the other samples at the same temperature.

Figure 12 displays the AC impedance spectroscopy of all BCZT samples measured at the temperature

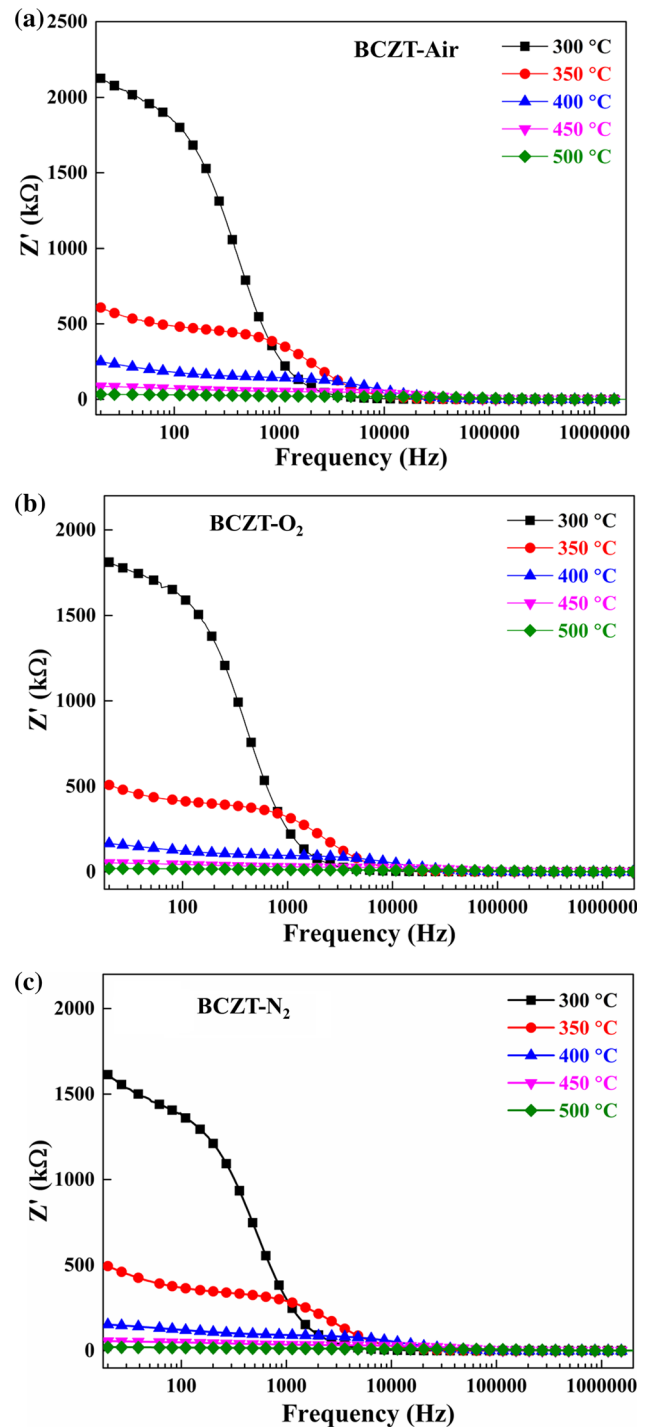


Figure 10 Frequency dependences of the Z' of samples measured at various temperatures: **a** BCZT-Air, **b** BCZT-O₂ and **c** BCZT-N₂.

range from 300 to 500 °C. The AC impedance spectroscopy of all BCZT samples gradually shows two semicircular arcs as the temperature rises, indicating that there are two different contributions to

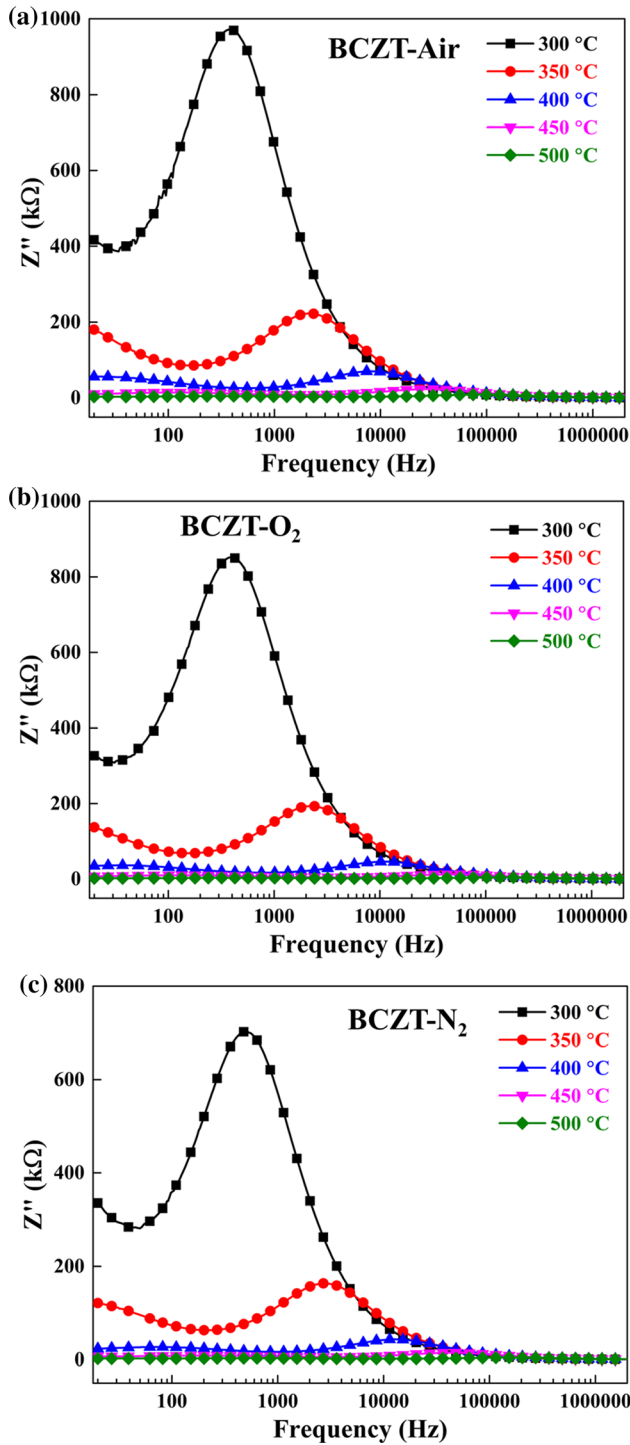


Figure 11 Z'' of the samples as a function of frequency measured at different temperatures: **a** BCZT-Air, **b** BCZT-O₂ and **c** BCZT-N₂.

impedance. The first semicircular arc at high frequency and the second semicircular arc at low frequency represent the function of the grain and grain boundary, respectively. It can be found that there is a

non-Debye type of relaxation process because the centers of the semicircles located below the real axis [61].

To obtain the resistance of grain (R_g), the capacitance of grain (CPE1), the resistance of grain

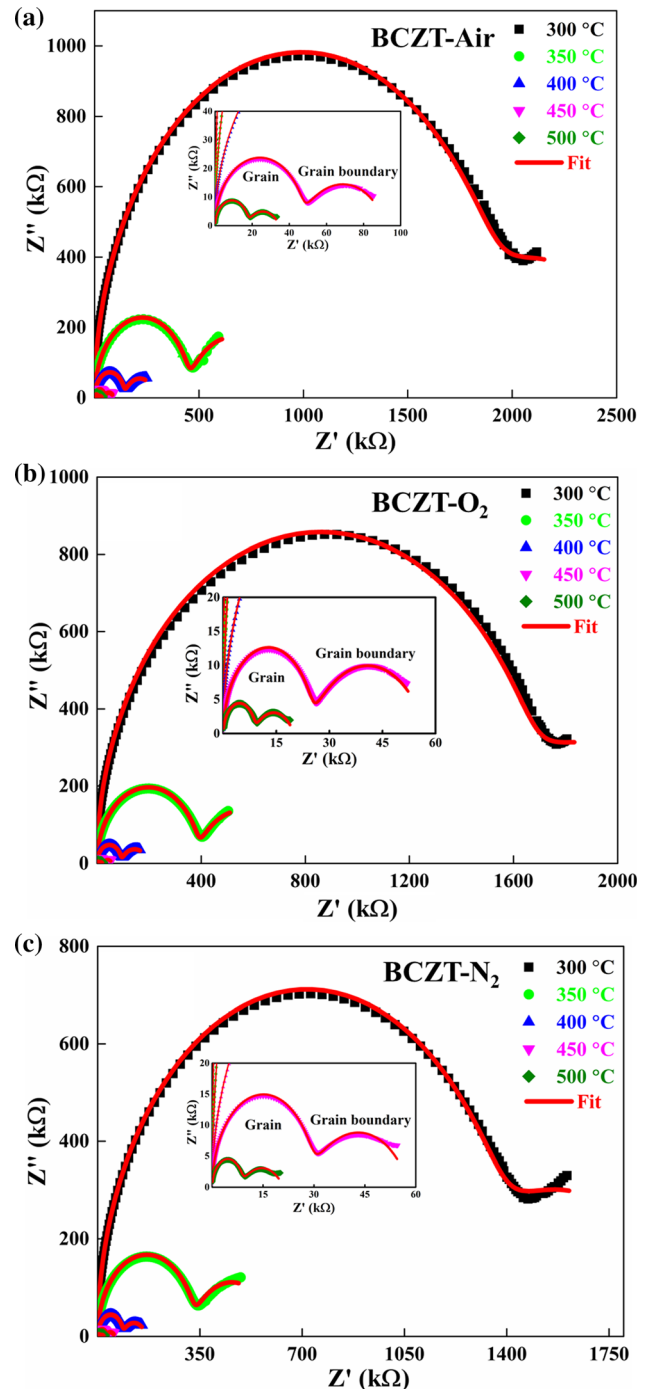


Figure 12 Complex impedance spectra of the samples measured at various temperatures: **a** BCZT-Air, **b** BCZT-O₂ and **c** BCZT-N₂.

boundary (R_{gb}) and the capacitance of grain boundary (CPE2), the Nyquist plots (Z' vs. Z'') of all BCZT ceramics were fitted by Z-view software, and the fitted results are shown in Fig. 12 (see red lines). The equivalent circuit diagram of CPE and R series parallel was used and is shown in Fig. 13. The conductivity (σ_g and σ_{gb}) of grain and grain boundary were obtained by $\sigma = \frac{1}{\rho} = \frac{t}{RS}$ (where σ represents the conductivity of the sample, ρ is the resistivity, t is the thickness of the sample, R is the resistance and S is the surface area of the sample). All obtained parameters are shown in Table 3. Firstly, the σ_g and σ_{gb} of all BCZT ceramics increase as the temperature rises, which shows obvious positive temperature coefficient characteristics [62]. Secondly, it is noteworthy that the conductivity of grain boundary is higher than that of grain in all BCZT ceramics measured at 300 °C, but the conductivity of grain boundary is relatively close to that of grain when the temperature is above 300 °C, which may be related to the generation or accumulation of defects such as oxygen vacancy. It has been reported that the transition temperature of some conduction mechanisms (such as electrons or holes) and oxygen vacancy conduction mechanism are around 300 °C in BCZT ceramics [62, 63]. In other words, the oxygen vacancy conduction mechanism may play a dominant role when the temperature is above 300 °C. Thirdly, according to the obtained resistance (R) and capacitance (CPE), the relaxation time (τ_g and τ_{gb}) of grain and grain boundary can be calculated by $\tau = R \times CPE$ (where R and CPE are the resistance and capacitance of sample, respectively) and is shown in Table 3. It is seen that τ_g and τ_{gb} gradually decrease as the temperature rises (except for 300 °C). The result indicates that the carrier mobility increases gradually as the temperature rises, which is because the carrier mobility is inversely proportional to the relaxation time [63]. The increased carrier mobility is due to that the carriers

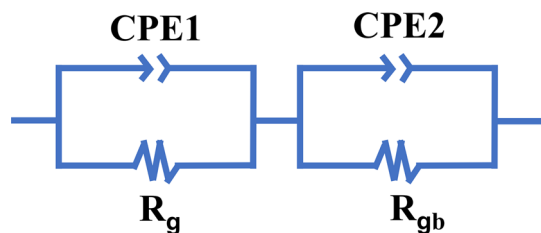


Figure 13 Equivalent circuit diagram of CPE and R series parallel.

(electron, hole or point defects) move more easily at the higher temperature. Moreover, the relaxation time of grain boundary (τ_{gb}) of all BCZT ceramics is much higher than that of grain (τ_g), suggesting that the carrier mobility of grain boundary is much lower. The result indicates that the defects such as oxygen vacancy ($V_O^{\bullet\bullet}$) migrate more easily in the grain. Finally, compared to BCZT-N₂ and BCZT-O₂ ceramics, BCZT-Air ceramics exhibit lower conductivity. As mentioned above, the oxygen vacancy concentration of BCZT samples sintered in O₂ is lower than that of BCZT samples sintered in air and N₂ according to EDS and XPS analysis. However, the conductivity of BCZT-O₂ ceramics is not the minimum among all samples. It is because that the conductivity depends on not only carrier concentration but also carrier mobility. The grain and grain boundary in BCZT-Air ceramics have greater relaxation time (τ) than BCZT-O₂ ceramics, suggesting BCZT-Air ceramics have lower carrier mobility than that of BCZT-O₂ ceramics. Therefore, although BCZT-Air ceramics have higher oxygen vacancy concentration than BCZT-O₂ ceramics, the lower carrier mobility of BCZT-Air ceramics plays a more important role and leads to lower conductivity. According to the same principle, BCZT-N₂ samples with the highest oxygen vacancy concentration and carrier mobility show the best conductivity among all the samples.

As everyone knows, there is usually the generation of oxygen vacancies during the high-temperature preparing process of oxide ceramics. The ionization of the oxygen vacancy ($V_O^{\bullet\bullet}$) simultaneously forms electrons, described by Kröger–Vink process [61]:



where V_O^{\bullet} and $V_O^{\bullet\bullet}$ represent the first and secondary ionization, respectively. In general, the lower oxygen vacancy concentration of the materials with perovskite structure corresponds to its higher activation energy (E_a) at high temperature [64]. Therefore, the activation energy of BCZT ceramics sintered in different atmospheres was calculated by Arrhenius law to find out the difference in oxygen vacancy content:

$$\sigma = \sigma_0 \exp\left(\frac{E_a}{K_B T}\right) \quad (5)$$

Table 3 Resistance (*R*), conductivity (σ), capacitance (CPE) and relaxation time (τ) of grain and grain boundary of all BCZT ceramics

Samples	<i>T</i> (°C)	<i>R</i> _g (kΩ)	σ _g (MΩ ⁻¹ ·cm ⁻¹)	CPE1 (nF)	τ _g (× 10 ⁻⁵ s)	<i>R</i> _{gb} (kΩ)	σ _{gb} (MΩ ⁻¹ ·cm ⁻¹)	CPE2 (nF)	τ _{gb} (× 10 ⁻² s)
BCZT-Air	300	1912	0.08	0.2128	40.7	859.2	0.18	24.8	2.13
	350	445.1	0.35	0.1661	7.39	443.2	0.35	54.21	2.40
	400	140.5	1.10	0.1397	1.96	155.1	1.00	96.04	1.49
	450	46.44	3.34	0.1257	0.58	45.62	3.40	198.3	0.90
	500	17.29	8.97	0.1217	0.09	17.27	8.98	415.6	0.72
BCZT-O ₂	300	1675	0.09	0.2186	36.62	559.5	0.28	30.74	1.72
	350	384.7	0.40	0.1832	7.05	351.3	0.44	71.43	2.51
	400	91.65	1.69	0.1534	1.41	106	1.46	138.1	1.46
	450	24.33	6.38	0.1342	0.33	33.3	4.66	308.8	1.03
	500	8.622	18.00	0.1393	0.12	11.29	13.74	662.5	0.75
BCZT-N ₂	300	1385	0.11	0.226	31.30	533.9	0.29	21.53	1.15
	350	325.6	0.48	0.1741	5.67	275.4	0.57	49.58	1.37
	400	85.17	1.85	0.1398	1.19	81.08	1.94	113.6	0.92
	450	28.63	5.49	0.1212	0.35	29.52	5.33	276.2	0.82
	500	8.446	18.61	0.1121	0.09	12.53	12.55	823.4	1.03

where σ represents the electrical conductivity, σ_0 represents the preexponential term, E_a represents the activation energy and K_B represents the Boltzmann constant. According to Eq. (5), the activation energy (E_a) of all BCZT ceramics was obtained by linear fitting (shown in Fig. 14). The E_a of grain and grain boundary of BCZT-Air, BCZT-O₂ and BCZT-N₂ samples are 0.942 eV and 0.813 eV, 1.023 eV and 0.953 eV, and 0.936 eV and 0.743 eV, respectively. According to the studies [62, 63, 65], the E_a of oxygen vacancy at secondary ionization (V_O^{**}) in BaTiO₃-based materials is between 0.6 eV and 1.28 eV. The E_a of our BCZT ceramics is good agreement with that of oxygen vacancy, which further confirms that the oxygen vacancy conduction mechanism of our BCZT samples dominates in the range of 300–500 °C and this is consistent with our previous hypothesis. Moreover, the highest activation energy of BCZT-O₂ ceramics suggests that it has the lowest oxygen vacancy concentration among all samples, which further supports the effects of oxygen atmosphere sintering. Based on similar principles, the lowest activation energy of BCZT-N₂ samples confirms its highest oxygen vacancy concentration.

Piezoelectric properties

To obtain the piezoelectric responses of BCZT samples, the unipolar electric field-induced strain (short for strain) curves, dynamic piezoelectric coefficient

($d_{33}^* = S_{max}/E_{max}$) (shown in Fig. 15), quasi-static piezoelectric coefficient d_{33} (shown in Fig. 17) and electromechanical coupling coefficient (k_p) were measured and are shown in Table 2. Figure 15 shows the strain and d_{33}^* of BCZT samples measured at various temperatures. Firstly, the strain and d_{33}^* of BCZT samples sintered in air, O₂ and N₂ at room temperature (25 °C) are 0.096% and 481.5 pm/V, 0.130% and 647.5 pm/V, and 0.125% and 627 pm/V, respectively, suggesting the most excellent piezoelectric responses of BCZT-O₂ samples. Secondly, the maximum strain and d_{33}^* of all BCZT samples first increase and then decrease as temperature rises, and the maximum strain and d_{33}^* of BCZT samples sintered in air, O₂ and N₂ are 0.110% and 549.5 pm/V, 0.136% and 684.5 pm/V, and 0.131% and 653.5 pm/V, respectively (shown in Fig. 15d–f). The corresponding temperature to the maximum strain and d_{33}^* of BCZT samples sintered in air, O₂ and N₂ is 32 °C, 30 °C and 28 °C, respectively, which is the same as T_{O-T} . The result confirms that the construction of the O-T phase boundary can significantly enhance the piezoelectric responses of BCZT samples, which is in accordance with the studies [13, 39]. In other words, if the transition temperature of the O–T phase in BCZT ceramics can shift to room temperature, the room-temperature piezoelectric responses can be significantly enhanced. Thirdly, the room-temperature strain of BCZT-O₂ samples is higher than that of BCZT-Air samples with the larger grain size, resulting from the phase boundary of the O–T phase closer

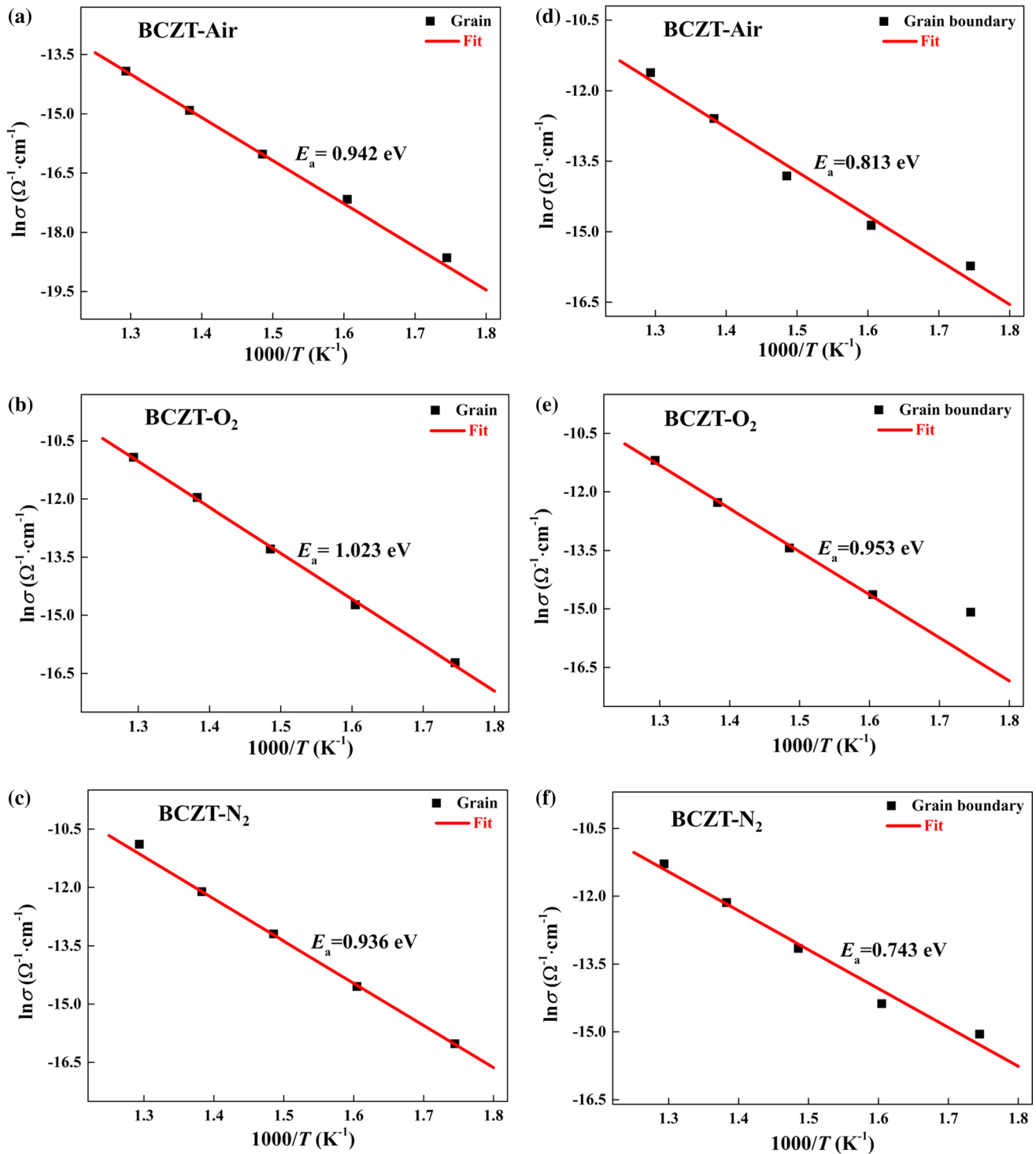


Figure 14 Arrhenius plots and the fitted activation energy (E_a) values of BCZT samples sintered in various atmospheres: **a, d** air, **b, e** O₂ and **c, f** N₂.

to room temperature in BCZT-O₂ ceramics. It is noteworthy that BCZT-O₂ ceramics still show the maximum piezoelectric response when all the samples are in the O–T phase boundary, which suggests

that the least oxygen vacancy and the best densification of BCZT-O₂ ceramics are also important factors affecting the piezoelectric response besides the construction of O–T phase boundary. The less oxygen

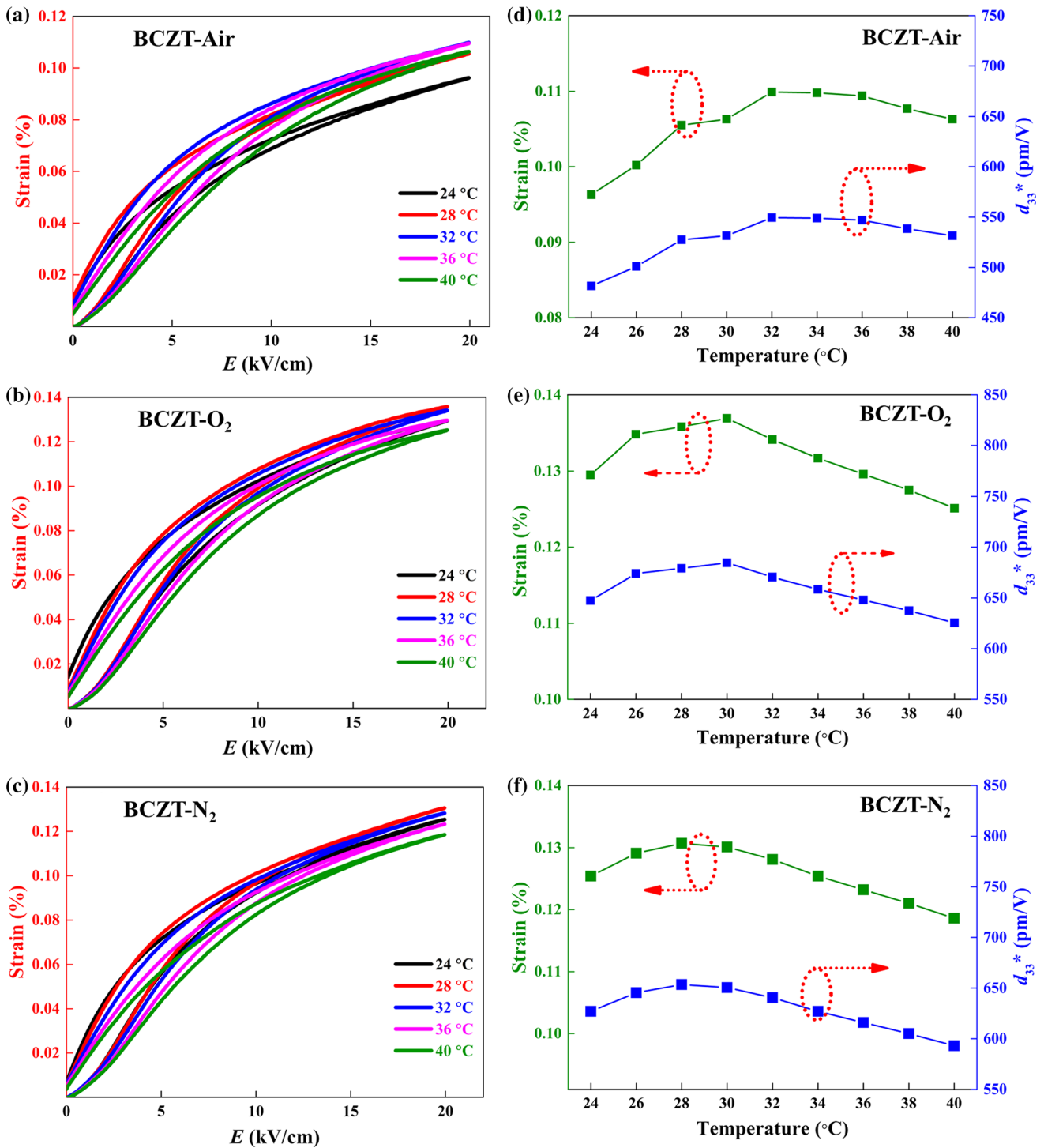


Figure 15 Strain and d_{33}^* of samples measured at various temperatures: **a, d** BCZT-Air, **b, e** BCZT-O₂ and **c, f** BCZT-N₂.

vacancy can weaken the pinning effect of the domain and make the domain easier to switch and then enhance the piezoelectric responses [66, 67]. Moreover, the relatively larger grain size exhibits less grain boundary volume, and the decreased grain boundary

results in the increase in the maximum field-induced strain so that the excellent piezoelectric response in piezoelectric ceramics with the larger grain size has been obtained [68, 69]. Based on the previous SEM, EDS, XPS and impedance spectroscopy, BCZT-O₂

ceramics have the best densification, larger grain size, the lowest oxygen vacancy concentration and O-T phase boundary near room temperature, which causes its most excellent piezoelectric responses. The piezoelectric responses of BCZT-N₂ samples are higher than those of BCZT-Air samples. Although BCZT-N₂ samples have more oxygen vacancy and smaller grain size than that of BCZT-Air samples, the piezoelectric response of BCZT-N₂ samples is superior to BCZT-Air samples. The result suggests that the effects of the O-T phase transition temperature closer to room temperature of BCZT-N₂ samples on piezoelectric response mask the anticipated effects of reduced grain size and increased oxygen vacancy. Meanwhile, the (001) orientation characteristics and uniform O-T phase coexistence of BCZT-N₂ samples could be the other reasons for its better piezoelectric properties. Finally, based on the above results, the phase diagram of BCZT samples sintered in different atmospheres was constructed and is given in Fig. 16.

Figure 17 shows the room-temperature d_{33} of all BCZT samples. Firstly, the d_{33} of BCZT samples sintered in air, O₂ and N₂ is 528.4 pC/N, 604.3 pC/N and 558.2 pC/N, respectively, further confirming that the piezoelectric responses of BCZT-O₂ ceramics are superior to the other ceramics. The result agrees with the strain behavior. Moreover, the electromechanical coupling coefficient k_p of BCZT samples sintered in air, O₂ and N₂ is 48%, 59% and 52%, respectively. In general, the piezoelectric properties originate from the intrinsic (lattice) and extrinsic (domain wall motions) contributions [70, 71]. The excellent

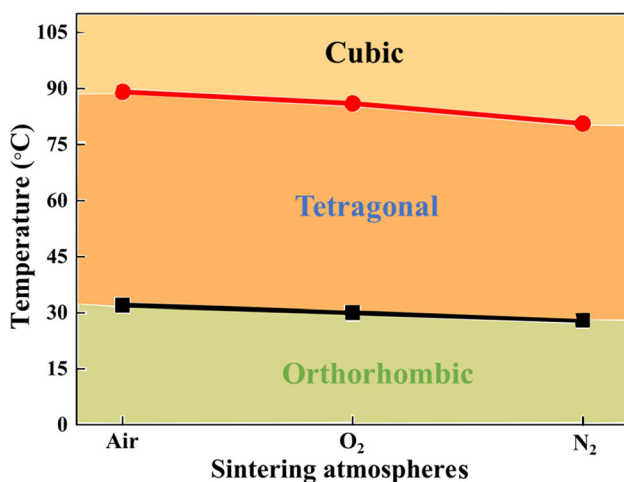


Figure 16 Phase diagram of BCZT samples sintered in various atmospheres.

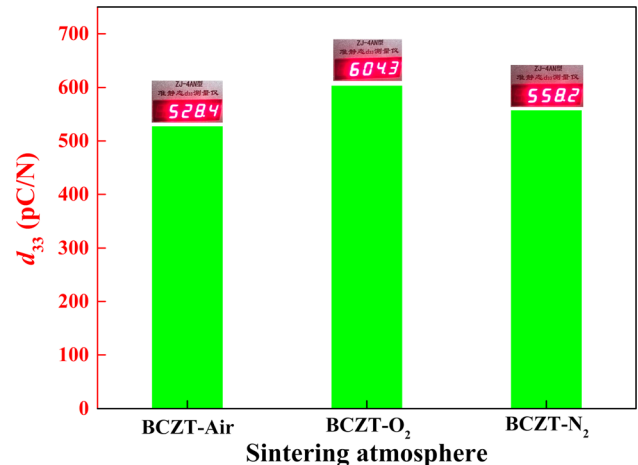


Fig. 17 Quasi-static piezoelectric coefficient (d_{33}) of BCZT ceramics.

piezoelectricity ($d_{33}^* = 647.5$ pm/V, $d_{33} = 604.3$ pC/N and $k_p = 59\%$) of BCZT-O₂ ceramics is related to the intrinsic contribution caused by the construction of O-T phase boundary (the coexistence of O-T phase) closer to room temperature and the extrinsic contribution caused by the high polarization which results from its relatively larger grain size and weakened domain wall pinning effect. The adjusting oxygen partial pressure in sintering is an effective approach to enhance the piezoelectric responses of BCZT ceramics, which has excellent developmental potential for actuator applications.

Conclusions

BCZT ceramics with enhanced piezoelectric responses have been successfully synthesized. BCZT ceramics sintered in air, O₂ and N₂ are the coexistence of orthorhombic and tetragonal phase at room temperature, but the content of phase coexistence is different, indicating that sintering atmosphere has significant influences on phase structure. The phase transition temperature of the O-T phase of BCZT ceramics sintered in air, O₂ and N₂ atmospheres is gradually closer to room temperature due to the combined action of internal stress and tetragonality. All BCZT ceramics sintered in various atmospheres exhibit distinct diffuse phase transition, and the diffuseness is enhanced with the refinement of grain. BCZT ceramics sintered in O₂ have the maximum P_r and the minimum E_C , which results from the decrease in oxygen vacancy and the shift of phase

transition temperature. The results of EDS, XPS and the activation energy confirm the lowest oxygen vacancy concentration of the ceramic sample sintered in O₂. The same mechanism caused by the decreased oxygen vacancy and shift of phase transition temperature makes BCZT ceramics sintered in O₂ achieve the improved piezoelectric responses ($d_{33} = 604.3$ pC/N and $d_{33}^* = 647.5$ pm/V).

Acknowledgements

This work was supported by the Excellent Talent Project in University of Chongqing (Grant No. 2017-35), the Program for Creative Research Groups in University of Chongqing (Grant No. CXQT19031), the Leading Talents of Scientific and Technological Innovation in Chongqing (Grant No. CSTCCXLJRC201919), the Innovation Program for Chongqing's Overseas Returnees (Grant No. cx2019159), the Chongqing Research Program of Basic Research and Frontier Technology (Grant No. CSTC2018jcyjAX0416), and the Chongqing Kehui Postgraduate Innovation and Entrepreneurship Project (Grant No. 09311065).

Compliance with ethical standards

Conflict of interest The authors and the institutes where the work has been carried out declare that there are no conflicts of interest regarding the publication of this article.

References

- [1] Hao JG, Li W, Zhai JW, Chen H (2019) Progress in high-strain perovskite piezoelectric ceramics. *Mat Sci Eng R* 135:1–57
- [2] Gao XY, Wu JG, Yu Y, Chu Z, Shi HD, Dong SX (2018) Giant piezoelectric coefficients in relaxor piezoelectric ceramic PNN-PZT for vibration energy harvesting. *Adv Funct Mater* 28:1706895
- [3] Shibata KJ, Wang RP, Tou T, Koruza J (2018) Applications of lead-free piezoelectric materials. *MRS Bull* 43:612–616
- [4] Zheng T, Wu JG, Xiao DQ, Zhu JG (2018) Recent development in lead-free perovskite piezoelectric bulk materials. *Prog Mater Sci* 98:552–624
- [5] Badapanda T, Sarangi S, Behera B, Sahoo PK, Anwar S, Sinha TP, Luz GE Jr, Longo E, Cavalcante LS (2014) Structural refinement, optical and ferroelectric properties of microcrystalline Ba(Zr_{0.05}Ti_{0.95})O₃ perovskite. *Curr Appl Phys* 14:708–715
- [6] Manjón-Sanz A, Berger C, Dolgos MR (2017) Understanding the structure–property relationships of the ferroelectric to relaxor transition of the (1 – x)BaTiO₃–xBiInO₃ lead-free piezoelectric system. *J Mater Sci* 52:5309–5323. <https://doi.org/10.1007/s10853-017-0770-x>
- [7] Shi J, Liu X, Tian WC (2019) Structure evolution and ferroelectric properties in stoichiometric Bi_{0.5+x}Na_{0.5-x}Ti_{1-0.5x}O₃. *J Mater Sci* 54:5249–5255. <https://doi.org/10.1007/s10853-018-03262-1>
- [8] Xi H, Yu LX, Hao Q, Chen FJ, Mao MM, Liu YF, Lyu YN (2020) Large strain with low hysteresis in Sn-modified Bi_{0.5}(Na_{0.75}K_{0.25})_{0.5}TiO₃ lead-free piezoceramics. *J Mater Sci* 55:1388–1398. <https://doi.org/10.1007/s10853-019-04154-8>
- [9] Yu ZD, Chen XM, Su YL, Lian HL, Lu JB, Zhou JP, Liu P (2019) Hot-press sintering K_{0.3}Na_{0.5}NbO₃–0.5 mol%Al₂O₃ ceramics with enhanced ferroelectric and piezoelectric properties. *J Mater Sci* 54:13457–13466. <https://doi.org/10.1007/s10853-019-03850-9>
- [10] Feng W, Cen ZY, Liang SY, Luo BC, Zhang Y, Zhen YC, Wang XH, Li LT (2019) Enhanced temperature stability of electric-field-induced strain in KNN-based ceramics. *J Alloy Compd* 786:498–506
- [11] Manjón-Sanz A, Culbertson CM, Hou D, Jones JL, Dolgos MR (2019) Total scattering and diffraction studies of lead-free piezoelectric (1 – x)Ba(Zr_{0.2}Ti_{0.8})O₃ – x(Ba_{0.7}Ca_{0.3})TiO₃ deconvolute intrinsic and extrinsic contributions to electromechanical strain. *Acta Mater* 171:79–91
- [12] Nahas Y, Akbarzadeh A, Prokhorenko S, Prosandeev S, Walter R, Kornev I, Íñiguez J, Bellaiche L (2017) Microscopic origins of the large piezoelectricity of leadfree (Ba, Ca)(Zr, Ti)O₃. *Nat Commun* 8:15944
- [13] Liu WF, Ren XB (2009) Large piezoelectric effect in Pb-free ceramics. *Phys Rev Lett* 103:257602
- [14] Castkova K, Maca K, Cihlar J, Hughes H, Matousek A, Tofel P, Bai Y, Button TW (2015) Chemical synthesis, sintering and piezoelectric properties of Ba_{0.85}Ca_{0.15}Zr_{0.1}Ti_{0.9}O₃ lead-free ceramics. *J Am Ceram Soc* 98:2373–2380
- [15] Li SB, Wang CB, Li L, Shen Q, Zhang LM (2018) Effect of annealing temperature on structural and electrical properties of BCZT ceramics prepared by plasma activated sintering. *J Alloy Compd* 730:182–190
- [16] Coondoo I, Panwar N, Alikin D, Bdikin I, Islam SS, Turygin A, Shur VY, Kholkin AL (2018) A comparative study of structural and electrical properties in lead-free BCZT ceramics: influence of the synthesis method. *Acta Mater* 155:331–342

- [17] Liu YC, Chang YF, Li F, Yang B, Sun Y, Wu J, Zhang ST, Wang RX, Cao WW (2017) Exceptionally high piezoelectric coefficient and low strain hysteresis in grain-oriented (Ba, Ca)(Ti, Zr)O₃ through integrating crystallographic texture and domain engineering. *ACS Appl Mater Inter* 9:29863–29871
- [18] Bai WF, Chen DQ, Li P, Shen B, Zhai JW, Ji ZG (2016) Enhanced electromechanical properties in $<001>$ -textured (Ba_{0.85}Ca_{0.15})(Zr_{0.1}Ti_{0.9})O₃ lead-free piezoceramics. *Ceram Int* 42:3429–3436
- [19] Jiang M, Lin Q, Lin DM, Zheng QJ, Fang XM, Wu XC, Sun HL, Wan Y, Wu L (2013) Effects of MnO₂ and sintering temperature on microstructure, ferroelectric, and piezoelectric properties of Ba_{0.85}Ca_{0.15}Ti_{0.90}Zr_{0.10}O₃ lead-free ceramics. *J Mater Sci* 48:1035–1041. <https://doi.org/10.1007/s10853-012-6835-y>
- [20] Zhou MX, Liang RH, Zhou ZY, Xu CH, Nie X, Dong XL (2018) Enhanced Curie temperature and piezoelectric properties of (Ba_{0.85}Ca_{0.15})(Zr_{0.10}Ti_{0.90})O₃ lead-free ceramics after the addition of LiTaO₃. *Mater Res Bull* 106:213–219
- [21] Guo FY, Cai W, Gao RL, Fu CL, Chen G, Deng XL, Wang ZH, Zhang QW (2019) Microstructure, enhanced relaxor-like behavior and electric properties of (Ba_{0.85}Ca_{0.15})(Zr_{0.1-x}Hf_xTi_{0.9})O₃ ceramics. *J Electron Mater* 48:3239–3247
- [22] Zhang Y, Sun HJ, Chen W (2018) A brief review of Ba(Ti_{0.8}Zr_{0.2})O₃-(Ba_{0.7}Ca_{0.3})TiO₃ based lead-free piezoelectric ceramics: past, present and future perspectives. *J Phys Chem Solids* 114:207–219
- [23] Liu Z, Yuan RH, Xue DZ, Cao WW, Lookman T (2018) Origin of large electrostrain in Sn⁴⁺ doped Ba (Zr_{0.2}Ti_{0.8})O₃-x(Ba_{0.7}Ca_{0.3})TiO₃ ceramics. *Acta Mater* 157:155–164
- [24] Wang P, Li YX, Lu YQ (2011) Enhanced piezoelectric properties of (Ba_{0.85}Ca_{0.15})(Ti_{0.9}Zr_{0.1})O₃ lead-free ceramics by optimizing calcination and sintering temperature. *J Eur Ceram Soc* 31:2005–2012
- [25] Wu JG, Xiao DQ, Wu WJ, Chen Q, Zhu JG, Yang ZC, Wang J (2011) Role of room-temperature phase transition in the electrical properties of (Ba, Ca)(Ti, Zr)O₃ ceramics. *Scripta Mater* 65:771–774
- [26] Hao JG, Bai WF, Li W, Zhai JW (2012) Correlation between the microstructure and electrical properties in high-performance (Ba_{0.85}Ca_{0.15})(Zr_{0.1}Ti_{0.9})O₃ lead-free piezoelectric ceramics. *J Am Ceram Soc* 95:1998–2006
- [27] Zhang QW, Cai W, Li QT, Gao RL, Chen G, Deng XL, Wang ZH, Cao XL, Fu CL (2019) Enhanced piezoelectric response of (Ba, Ca)(Ti, Zr)O₃ ceramics by super large grain size and construction of phase boundary. *J Alloy Compd* 794:542–552
- [28] Yan XD, Zheng MP, Sun SJ, Zhu MK, Hou YD (2018) Boosting energy harvesting performance in (Ba, Ca)(Ti, Zr)O₃ lead-free perovskites through artificial control of intermediate grain size. *Dalton T* 47:9257–9266
- [29] Zhao HD, Ma WB, Guo JD, Zang XR, Miao PS, Ma MJ, Zhang FY (2018) Low temperature sintering and role of room-temperature phase transition in the electrical properties of (Ba_{0.85}Ca_{0.15})(Zr_{0.10}Ti_{0.90})_{1-x}(Cu_{1/3}Nb_{2/3})_xO₃ ceramics. *J Mater Sci-Mater El* 29:2949–2957
- [30] Wu YH, Ma F, Qu JK, Luo Y, Song J, Wei GY, Zhang YC, Qi T (2018) Role of Cu and Y in sintering, phase transition, and electrical properties of BCZT lead-free piezoceramics. *Ceram Int* 44:15001–15009
- [31] Zhang J, Hou YD, Zheng MP, Jia WX, Zhu MK, Yan H (2016) The occupation behavior of Y₂O₃ and its effect on the microstructure and electric properties in X7R dielectrics. *J Am Ceram Soc* 99:1375–1382
- [32] Zheng MP, Hou YD, Xie FY, Chen J, Zhu MK, Yan H (2013) Effect of valence state and incorporation site of cobalt dopants on the microstructure and electrical properties of 0.2PZN–0.8PZT ceramics. *Acta Mater* 61:1489–1498
- [33] Zhang SW, Zhang HL, Zhang BP, Zhao GL (2009) Dielectric and piezoelectric properties of (Ba_{0.95}Ca_{0.05})(Ti_{0.88}Zr_{0.12})O₃ ceramics sintered in a protective atmosphere. *J Eur Ceram Soc* 29:3235–3242
- [34] Zhao LY, Hou YD, Wang C, Zhu MK, Yan H (2009) The enhancement of relaxation of 0.5PZN-0.5PZT annealed in different atmospheres. *Mater Res Bull* 44:1652–1655
- [35] Fan HQ, Park GT, Choi JJ, Kim HE (2001) Effect of annealing atmosphere on domain structures and electromechanical properties of Pb(Zn_{1/3}Nb_{2/3})O₃-based ceramics. *Appl Phys Lett* 79:1658–1660
- [36] Ji X, Wang CB, Zhang S, Tu R, Shen Q, Shi J, Zhang LM (2019) Structural and electrical properties of BCZT ceramics synthesized by sol-gel-hydrothermal process at low temperature. *J Mater Sci Mater El* 30:12197–12203
- [37] Chandrakala E, Praveen JP, Hazra BK, Das D (2016) Effect of sintering temperature on structural, dielectric, piezoelectric and ferroelectric properties of sol-gel derived BZT-BCT ceramics. *Ceram Int* 42:4964–4977
- [38] Ma CL, Wang XY, Gan ZX, Tan WS, Wang XX, Zhang J, Zhou WP (2019) Photoluminescence and optical temperature sensing in Sm³⁺ doped Ba_{0.85}Ca_{0.15}Ti_{0.90}Zr_{0.10}O₃ lead-free ceramics. *Ceram Int* 45:588–594
- [39] Yan XD, Zheng MP, Hou YD, Zhu MK (2017) Composition-driven phase boundary and its energy harvesting performance of BCZT lead-free piezoelectric ceramic. *J Eur Ceram Soc* 37:2583–2589

- [40] Zhao ZH, Li XL, Dai YJ, Ji HM, Su D (2016) Highly textured $\text{Ba}_{0.85}\text{Ca}_{0.15}\text{Ti}_{0.90}\text{Zr}_{0.10}\text{O}_3$ ceramics prepared by reactive template grain growth process. *Mater Lett* 165:131–134
- [41] Zhao ZH, Li XL, Dai YJ, Ye MY, Ji HM (2016) Texture development in $\text{Ba}_{0.85}\text{Ca}_{0.15}\text{Ti}_{0.90}\text{Zr}_{0.10}\text{O}_3$ lead-free ceramics prepared by reactive template grain growth with different Ba and Ca sources. *Ceram Int* 42:18756–18763
- [42] Yang CH, Sui HT, Wu HT, Hu GD (2015) $\text{Na}_{0.5}\text{Bi}_{0.5}(\text{Ti}_{0.98}\text{Zr}_{0.02})\text{O}_3$ thin film with improved performance by modifying annealing atmosphere and Zr doping content. *J Alloy Compd* 637:315–320
- [43] Zhang FQ, Zhang LP, Guo XD, Yang SJ, Tian QB, Fan SH (2018) The effect of sintering atmospheres on the properties of CSBT-0.15 ferroelectric ceramics. *Ceram Int* 44:13502–13506
- [44] Chen XM, Hu GD, Yan J, Wang X, Yang CH, Wu WB (2008) Enhanced multiferroic properties of (110)-oriented BiFeO_3 film deposited on $\text{Bi}_{3.5}\text{Nd}_{0.5}\text{Ti}_3\text{O}_{12}$ -buffered indium tin oxide/Si substrate. *J Phys D Appl Phys* 41:225402
- [45] Tkach A, Okhay O, Almeida A, Vilarinho PM (2017) Giant dielectric permittivity and high tunability in Y-doped SrTiO_3 ceramics tailored by sintering atmosphere. *Acta Mater* 130:249–260
- [46] Zhang L, Yao ZH, Lanagan MT, Hao H, Xie J, Xu Q, Yuan MX, Sarkarat M, Cao MH, Liu HX (2018) Effect of oxygen treatment on structure and electrical properties of Mn-doped $\text{Ca}_{0.6}\text{Sr}_{0.4}\text{TiO}_3$ ceramics. *J Eur Ceram Soc* 38:2534–2540
- [47] Reddy SR, Prasad VVB, Bysakh S, Shanker V, Hebalkar N, Roy SK (2019) Superior energy storage performance and fatigue resistance in ferroelectric BCZT thin films grown in an oxygen-rich atmosphere. *J Mater Chem C* 7:7073–7082
- [48] Bijalwan V, Tofel P, Erhart J, Maca K (2019) The complex evaluation of functional properties of nearly dense BCZT ceramics and their dependence on the grain size. *Ceram Int* 45:317–326
- [49] Liu YW, Pu YP, Sun ZX (2014) Enhanced relaxor ferroelectric behavior of BCZT lead-free ceramics prepared by hydrothermal method. *Mater Lett* 137:128–131
- [50] Frey MH, Payne DA (1996) Grain-size effect on structure and phase transformations for barium titanate. *Phys Rev B* 54:3158
- [51] Martirena HT, Burfoot JC (1974) Grain-size effects on properties of some ferroelectric ceramics. *J Phys C: Solid State Phys* 7:3182
- [52] Buessem WR, Cross LE, Goswami AK (1992) Phenomenological theory of high permittivity in fine-grained barium titanate. *J Am Ceram Soc* 75:2923–2926
- [53] Sharma P, Kumar P, Kundu RS, Juneja JK, Ahlawat N, Punia R (2015) Structural and dielectric properties of substituted barium titanate ceramics for capacitor applications. *Ceram Int* 41:13425–13432
- [54] Lin YT, Miao XR, Qin N, Zhou H, Deng WL, Bao DH (2012) Effects of Mn doping on structural and dielectric properties of sol-gel-derived $(\text{Ba}_{0.835}\text{Ca}_{0.165})(\text{Zr}_{0.09}\text{Ti}_{0.91})\text{O}_3$ thin films. *Thin Solid Films* 520:5146–5150
- [55] Haertling GH (1999) Ferroelectric ceramics: history and technology. *J Am Ceram Soc* 82:797–818
- [56] Leu CC, Chen C, Chien CH, Chang MN (2003) Domain structure study of $\text{SrBi}_2\text{Ta}_2\text{O}_9$ ferroelectric thin films by scanning capacitance microscopy. *Appl Phys Lett* 82:3493–3495
- [57] Kaddoussi H, Gagou Y, Lahmar A, Belhadi J, Allouche B, Dellis JL, Courty M, Khemakhem H, Marssi ME (2015) Room temperature electro-caloric effect in lead-free $\text{Ba}(\text{Zr}_{0.1}\text{Ti}_{0.9})_{1-x}\text{Sn}_x\text{O}_3$ ($x = 0, x = 0.075$) ceramics. *Solid State Commun* 201:64–67
- [58] Lee JW, Koh JH (2015) Grain size effects on the dielectric properties of $\text{CaCu}_3\text{Ti}_4\text{O}_{12}$ ceramics for supercapacitor applications. *Ceram Int* 41:10442–10447
- [59] Liu BB, Wang XH, Zhang RX, Li LT (2017) Grain size effect and microstructure influence on the energy storage properties of fine-grained BaTiO_3 -based ceramics. *J Am Ceram Soc* 100:3599–3607
- [60] Jha AK (2013) Electrical characterization of zirconium substituted barium titanate using complex impedance spectroscopy. *Bull Mater Sci* 36:135–141
- [61] Wang XF, Liang PF, Chao XL, Yang ZP (2015) Dielectric properties and impedance spectroscopy of MnCO_3 -modified $(\text{Ba}_{0.85}\text{Ca}_{0.15})(\text{Zr}_{0.1}\text{Ti}_{0.9})\text{O}_3$ lead-free ceramics. *J Am Ceram Soc* 98:1506–1514
- [62] Rafiq MA, Rafiq MN, Saravanan KV (2015) Dielectric and impedance spectroscopic studies of lead-free barium-calcium-zirconium-titanium oxide ceramics. *Ceram Int* 41:11436–11444
- [63] Coondoo I, Panwar N, Vidyasagar R, Kholkin AL (2016) Defect chemistry and relaxation processes: effect of an amphoteric substituent in lead-free BCZT ceramics. *Phys Chem Chem Phys* 18:31184–31201
- [64] Steinsvik S, Bugge R, Gjonnes J, Taftø J, Norby T (1997) The defect structure of $\text{SrTi}_{1-x}\text{Fe}_x\text{O}_{3-y}$ ($x = 0-0.8$) investigated by electrical conductivity measurements and electron energy loss spectroscopy (EELS). *J Phys Chem Solids* 58:969–976
- [65] Sindhu M, Ahlawat N, Sanghi S, Kumari R, Agarwal A (2013) Effect of Zr substitution on phase transformation and dielectric properties of ceramics. *J Appl Phys* 114:164106
- [66] Zhao ZH, Li X, Ji HM, Dai YJ, Li T (2015) Microstructure and electrical properties in Zn-doped $\text{Ba}_{0.85}\text{Ca}_{0.15}\text{Ti}_{0.90}\text{Zr}_{0.10}\text{O}_3$ piezoelectric ceramics. *J Alloy Compd* 637:291–296
- [67] Lu HW, Liu LZ, Lin JQ, Yang WL, Weng L, Zhang XR (2018) Effects of Tb doping on structural and electrical properties of $0.47(\text{Ba}_{0.7}\text{Ca}_{0.3})\text{TiO}_3-0.53\text{Ba}(\text{Zr}_{0.2}\text{Ti}_{0.8})\text{O}_3$ thin

- films at various annealing temperature by pulsed laser deposition. *Ceram Int* 44:6514–6519
- [68] Tan YQ, Zhang JL, Wang CL, Viola G, Yan HX (2015) Enhancement of electric field-induced strain in BaTiO₃ ceramics through grain size optimization. *Phys Status Solidi A* 212:433–438
- [69] Cao WW (2005) Ferroelectrics: the strain limits on switching. *Nat Mater* 4:727
- [70] Leontsev SO, Eitel RE (2011) Origin and magnitude of the large piezoelectric response in the lead-free (1-x)BiFeO₃-xBaTiO₃ solid solution. *J Mater Res* 26:9–17
- [71] Zhao CH, Hou D, Chung CC, Zhou HH, Kynast A, Hennig E, Liu WF, Li ST, Jones JL (2018) Deconvolved intrinsic and extrinsic contributions to electrostrain in high performance, Nb-doped Pb(Zr_xTi_{1-x})O₃ piezoceramics (0.50 ≤ x ≤ 0.56). *Acta Mater* 158:369–380

Publisher's Note Springer Nature remains neutral with regard to jurisdictional claims in published maps and institutional affiliations.